

Transient chaotic dimensionality expansion by recurrent networks

Christian Keup,^{1,2,*} Tobias Kühn,^{1,2,3,*} David Dahmen,¹ and Moritz Helias^{1,4}

¹*Institute of Neuroscience and Medicine (INM-6) and Institute for Advanced Simulation (IAS-6) and JARA
Institut Brain Structure-Function Relationships (INM-10), Jülich Research Centre, Jülich, Germany*

²*RWTH Aachen University, Aachen, Germany*

³*Laboratoire de Physique Théorique de l'ENS and CNRS, Paris, France*

⁴*Department of Physics, Faculty 1, RWTH Aachen University, Aachen, Germany*

(Dated: December 21, 2024)

ABSTRACT

Cortical neurons communicate with spikes, which are discrete events in time. Functional network models often employ rate units that are continuously coupled by analog signals. Is there a benefit of discrete signaling? By a unified mean-field theory for large random networks of rate and binary units, we show that the two models have identical second order statistics. Their stimulus processing properties, however, are radically different: We discover a chaotic sub-manifold in binary networks that does not exist in rate models. Its dimensionality increases with time after stimulus onset and reaches a fixed point that depends on the synaptic coupling strength. Low dimensional stimuli are transiently expanded into higher-dimensional representations that live within the manifold. We find that classification performance peaks within a single neurons' activation. High noise resilience persists not only near the edge of chaos, but throughout the chaotic regime. In rate models of spiking activity, the effective spiking noise suppresses chaos and results in negligible classification performance. For chaotic rate networks without effective spiking noise, the transient performance boost can also be identified. The transition to chaos in the two models do not coincide and have qualitatively different causes. Our theory mechanistically explains these observations.

These findings have several implications. 1) Optimal performance is reached with weaker synapses in discrete state networks compared to rate models; implying lower energetic costs for synaptic transmission. 2) The classification mechanism is robust to noise, compatible with fluctuations in biophysical systems. 3) Optimal performance is reached after only a single activation per participating neuron; this demonstrates efficient event-based computation with short latencies. 4) The presence of a chaotic sub-manifold has implications for the variability of neuronal activity; the theory predicts a transient increase of variability after stimulus onset. Our results thus provide a hitherto unknown link between recurrent and chaotic dynamics of functional networks, neuronal variability, and dimensionality of neuronal responses.

I. INTRODUCTION

Random networks of simplified neurons have been extensively studied to explain the asynchronous, irregular spiking activity observed in cortical networks [1–7]. It is a long standing question in how far information processing in cortex is based on the exact spike times of its neurons, or whether the high convergence of many input spike trains onto a neuron results in an effectively averaged spike rate that conveys the information [8–12]. In this case, variability of the exact spike time realizations can be treated as discretization noise on an actually continuous signal, while in the first case the 'noise' carries elaborate internal dependencies that encode information. Random networks were at first used mainly to describe the activity statistics and not computation. However, it was found that the computational capabilities of a network are highest in a regime where the activity is close to the border between regular and chaotic dynamics [13–15], and such a transition exists in random networks of (continuous-valued) rate neurons [16]. It is an ongoing debate and open question, in how far this transition to chaos in rate models translates to the behavior of spiking models [17–22]. This question is interrelated with the question of discrete versus continuous coding in cortex: Firstly, if cortex employs a discrete code, one expects computation to peak at the transition to chaos on the level of spike times; it is, however, not clear why this transition should coincide with or be similar to the onset of chaotic fluctuations in a rate model, where no notion of spike times exists. In particular, infinitely large random spiking networks are expected to be always chaotic [2, 23] which is not the case for rate models; the latter exhibit a transition between regular and chaotic dynamics depending on coupling strength [16, 18, 24] and noise amplitude [25, 26]. Second, if cortex employs a rate code, the spike rates should be close to a chaotic instability, but the realization of individual spike times is expected to be fully chaotic, constituting a discretization noise that would affect the susceptible spike rates and could change the network's computational properties. Here, we hope to make a contribution towards an answer of this question.

To do so, we study two types of random networks: The first employs a neuron model where cells communicate by continuous-valued signals. The second uses communication with discrete-valued signals among cells. To isolate the effect of discrete versus continuous communication,

* C.K. and T.K. contributed equally to this work.

we first develop a unified framework that has the same mathematical structure for the two models.

This approach allows us to understand which network properties generalize across model classes and which are distinct features of either class. In general, investigating the links between different neuron models holds the prospect of better integrating and comparing results known only for specific models among the large diversity of existing neuron models.

As the continuous model, our choice are noisy nonlinear rate neurons, for which the chaos transition in random networks is known analytically [16, 26]. As the discrete model, we use stochastic binary neurons with asynchronous updates. In the model hierarchy, binary neurons can be considered as in between rate neurons and spiking neurons, such as the leaky-integrate-and-fire (LIF) model. They explicitly reflect the threshold-like nonlinearity that is characteristic of deterministic spiking neurons and our feature of interest, while taking the memory effect of the leaky membrane voltage into account stochastically through the timescale of their update process. We here show that the transition to chaos in either model can be reduced to the question of how a pair of neurons transmits pairwise correlations between their input to their output. This relation then exposes a qualitative similarity between the chaotic behavior of the LIF model and its abstraction as a binary model. Since LIF neurons are more difficult to treat analytically, it is advantageous to use binary neurons as the simpler model. We show that, despite the qualitative differences between the rate and binary models, one can construct networks that in fact exhibit exactly identical activity statistics. This allows us to study their distinct computational properties that solely result from the difference of continuous versus discretized signal transmission.

In the seminal works by Sompolinsky *et al.* [16] on rate neurons and by van Vreeswijk and Sompolinsky [27] on binary neurons different approaches were used. While derivations in Sompolinsky *et al.* [16] were based on statistical field theory [24], those on binary networks in van Vreeswijk and Sompolinsky [27] used a disorder average of the master equation as a starting point [1, 28]. Here we develop a common field theoretical approach that captures both models, which is similar to the MSRDJ [29, 30] formalism for rate neurons [reviewed e.g. in 31, 32]. The formulation of binary neurons in a path integral is nontrivial due to the non-equilibrium dynamics resulting from asymmetric connectivity, so that the Ising Hamiltonian cannot be used. Instead, complete information about the system dynamics is required to write down a closed form action. For rate neurons this is supplied by the differential equation governing the dynamics which is amenable to the MSRDJ method. For binary neurons, full information is supplied by the Master equation, for which an existing approach is the Doi-Peliti formalism [33, 34]. The appearing fields have a convoluted physical interpretation, but allow to construct mean field equations and fluctuation corrections [35–37].

Our approach is drastically different: instead of demanding an explicit closed form of the action, we only require the output of a neuron given its input as a conditional probability. We then exploit that when calculating a quantity in a given approximation, only partial knowledge needs to be actually inserted. In this way, our field theoretical framework is flexible enough to cover both model classes with identical sets of physically interpretable fields. This common language thus provides a systematic way of calculating corresponding quantities in the same approximation for both models.

Averaging over the different sources of quenched disorder, we recover the known dynamical mean field theory (DMFT) equations for networks of binary neurons and then show that, surprisingly, they are equivalent to the DMFT equations for the noisy rate model. As a result of this unification, for each network of binary neurons, a rate network can be found with exactly the same first and second order statistics. In light of the close correspondence between the two models, we proceed to ask the question in how far the chaotic behavior is also similar.

By a replica calculation that determines the divergence or convergence of nearby trajectories, we here show that the behavior is very different in the two models. Especially, in the thermodynamic limit, binary networks are always chaotic while their statistically matched rate counterparts are not. Being interested in finite networks however, we find that the theory predicts a chaos transition in binary networks that strongly depends on the network size. This transition has no correspondence to the size-independent chaos transition in rate networks. This is explainable in terms of the difference between the internal generation of the binary discretization compared to the independent realization of the external noise of the rate models.

Lastly, we analyze implications for computation at the two edges of chaos of either model. Both theoretically and by simulation we show that beyond the edge of chaos, the dynamics of the binary network is governed by an attractive chaotic sub-manifold. In a noisy pattern classification task, the informative signal expands into this manifold faster than its noise, resulting in a transient dimensionality expansion of the signal that improves the classification performance.

Results in Section II are organized as follows. In Section II A we present the model-independent field-theory for random networks and resulting equations for mean activities. Section II B derives equivalent equations for autocorrelations in binary and rate networks which allow us in Section II C to find a mapping of parameters between the two models to obtain identical mean-field statistics. Section II D shows that binary networks are always chaotic in the thermodynamic limit $N \rightarrow \infty$ and exposes the relation between correlation transmission and chaotic transition. Section II E shows that finite-size binary networks in fact show transition to chaos and expose the existence of a finite-dimensional chaotic sub-manifold. Section II F investigates the con-

sequence for computation in chaotic binary networks, showing that a fast, transient dimensionality expansion of presented stimuli takes place within the chaotic sub-manifold. Section II G exposes the difference to computation in rate networks.

II. RESULTS

A. Model-independent field-theory of neuronal networks

We here derive a framework to compute the statistics of neuronal networks in a manner that is largely independent of the employed neuron model. Such a framework is needed to compare the different model classes. It must be flexible enough to enable the use of methods such as disorder averages and replica calculations; techniques that are required to systematically derive mean-field equations and to compute the phase diagram of neuronal networks.

We consider a network of N neurons with connectivity matrix \mathbf{J} , where individual entries are drawn independently and identically distributed as $J_{ij} \stackrel{\text{i.i.d.}}{\sim} \mathcal{N}\left(\frac{\bar{g}}{N}, \frac{g^2}{N}\right)$; assumptions on the statistics can easily be relaxed. The N neurons have inputs $\mathbf{h} = (h_1(t), \dots, h_N(t))$ and outputs $\mathbf{x} = (x_1(t), \dots, x_N(t))$. Throughout, bold-font symbols will be used to denote vectors of neuron indices. The input-to-output relation of a neuron is often stochastic, so that a conditional probability $\rho[\mathbf{x}|\mathbf{h}]$ of the output given the input describes the neural dynamics. The joint statistics of input and output is then

$$\rho[\mathbf{x}, \mathbf{h}] = \rho[\mathbf{x}|\mathbf{h}] \rho[\mathbf{h}], \quad (1)$$

amounting to a separation of the neurons' input-output functional $\rho[\mathbf{x}|\mathbf{h}] := \prod_i \rho[x_i|h_i]$ and the input statistics $\rho[\mathbf{h}]$. We here denote functionals by angular brackets.

We can express any observable O of a neuronal network as a function of the inputs \mathbf{h} , which have the advantage to be closer to a Gaussian distribution than \mathbf{x} , due to the convergence of many outputs on one input. Because we do not know the disorder realization (e.g. of the connectivity) in detail, but at most its statistics, we can only access quenched disorder-averaged quantities like

$$\langle O[\mathbf{h}] \rangle_{J, \mathbf{h}} := \int \mathcal{D}\mathbf{h} \langle \rho[\mathbf{h}](\mathbf{J}) \rangle_J O[\mathbf{h}].$$

The description of the network dynamics is self-consistently closed by using a delta distribution $\rho[\mathbf{h}] = \delta[\mathbf{h} - \mathbf{J}\mathbf{x}]$ to enforce that the input to each neuron is composed of a sum of outputs weighted by the synaptic connectivity \mathbf{J} . This idea is illustrated in Figure 1a. Note that (1) is not a circular definition because $\rho[\mathbf{x}|\mathbf{h}]$ is a causal functional and $\rho[\mathbf{h}]$ only couples equal time points, so that the concatenation in (1) can be understood as a spiral moving forward in time.

Using the Fourier-representation of $\rho[\mathbf{h}]$ we obtain, at the expense of introducing the response fields $\hat{\mathbf{h}}$, the

disorder-averaged input statistics

$$\begin{aligned} \langle \rho[\mathbf{h}](J) \rangle_J &= \left\langle \int \mathcal{D}\mathbf{x} \rho[\mathbf{x}, \mathbf{h}] \right\rangle_J \\ &= \int \mathcal{D}\hat{\mathbf{h}} \exp\left(\hat{\mathbf{h}}^T \mathbf{h}\right) \\ &\quad \times \int \mathcal{D}\mathbf{x} \left\langle \exp\left(-\hat{\mathbf{h}}^T \mathbf{J}\mathbf{x}\right) \right\rangle_J \rho[\mathbf{x}|\mathbf{h}], \end{aligned}$$

being similar as in [38–40]. The connectivity average only acts on the interaction term, which now has the form of a cumulant generating function of \mathbf{J} . In its cumulant expansion, intensive parameters of the system are the first and second cumulant \bar{g}/N and g^2/N , respectively. Higher cumulants would be suppressed if one assumes the commonly chosen scaling $\propto N^{-\frac{1}{2}}$ of synaptic weights [2, 27].

This suggests to do a Hubbard-Stratonovich transformation with the auxiliary fields $\mathcal{R}(t) := \frac{\bar{g}}{N} \sum_i x_i(t)$ and $\mathcal{Q}(t, s) := \frac{g^2}{N} \sum_i x_i(t)x_i(s)$, as outlined in appendix Section 1, so that a saddle point approximation gives self-consistency relations for the mean inputs and mean time lagged autocorrelations of dynamical mean field theory (DMFT)

$$R(t) = \bar{g} \langle x(t) \rangle_{\Omega(R, Q)}, \quad (2)$$

$$Q(t, s) = g^2 \langle x(t)x(s) \rangle_{\Omega(R, Q)}, \quad (3)$$

where the average $\langle \dots \rangle_{\Omega(R, Q)}$ is defined in (27) as an average over $x \sim \langle \rho[x|\mathbf{h}] \rangle_{\mathbf{h}}$ and \mathbf{h} is a Gaussian process $\mathbf{h} \sim \mathcal{N}(R, Q)$. We may think of $x(t)$ as the representative neuron of a homogeneous population, because all neurons with statistically identical connectivity and properties are identical after the disorder average. On the intuitive level, DMFT corresponds to modeling the inputs of all neurons as independent Gaussian processes $\mathbf{h} \sim \mathcal{N}(R, Q)$.

Thus, it was possible to formally derive the DMFT using only the output-to-input relation given by the disordered connectivity while staying agnostic of the neuron model. To instantiate the approximation for the models studied here, we must now provide knowledge about the input-to-output relation $\rho[\mathbf{x}|\mathbf{h}]$ of each model.

Binary neuron model We first consider the binary neuron model, or kinetic Ising model, with state $x_i \in \{-1, 1\}$ [1, 28]. The states of all neurons are updated asynchronously by independent Poisson processes with rate τ^{-1} and an activation probability function $T_p: \mathbb{R} \rightarrow [0, 1]$. It is clear that the form of $\rho[\mathbf{x}|\mathbf{h}]$ depends on the realization of the update times, which constitute a source of noise, or temporal stochasticity. The update sequence may be thought of as another type of disorder in a sense that it breaks the homogeneity of the time axis by selecting a set of time points where the neuronal state can change. As with the disorder of the connectivity one may study the behavior of the system averaged across this disorder. In this case, the probability of finding a neuron active at some time t

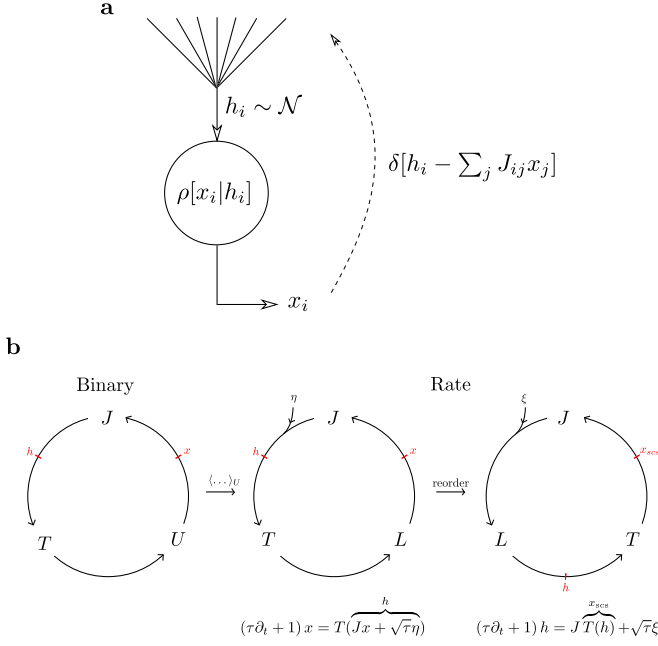


Figure 1. Summary of model-independent field theory and mapping of binary and rate models. **a** Conceptual idea to split network into neuronal dynamics, described by conditional probability $\rho[x_i|h_i]$ of neuronal output x_i given its input h_i , and the mapping of output to input by connectivity J_{ij} . The connectivity average only affects the output-to-input mapping and can thus be performed without specifying the neuron model. The formal saddle point approximation in auxiliary fields $\mathcal{R}(t)$ and $\mathcal{Q}(t, s)$, eqs. (3) and (3), amounts to Gaussian approximation of the input h_i . **b** Equivalence of binary (left) and rate models in the two different forms (6) (middle) and (7) (right): Mapping from output to input by identical matrix J ; asynchronous update process U with rate τ^{-1} implies exponential convolution kernel, leading to leaky-integration (cf. (4)), identical to operator $L = (\tau\partial_t + 1)^{-1}$ present explicitly in (6) and (7). Transitions between discrete binary states effect red noise η in input h (middle), which corresponds to white noise ξ that is low-pass filtered by L (right). Rate models differ in the order of application of this kernel and the connectivity, which yields equivalent dynamics because the two operators commute.

is $p[x_i(t) = 1|h_i] = \int_{-\infty}^t \frac{dt'}{\tau} e^{-\frac{t-t'}{\tau}} T_p(h_i(t'))$. While this knowledge is far from knowing the complete probability functional $\rho[\mathbf{x}|\mathbf{h}]$ across its infinite time dimension, the information about this single time slice is sufficient to plug into (3) and obtain, after taking a time derivative, the mean field equation

$$\tau \frac{d}{dt} R(t) + R(t) = \bar{g} \langle T(h(t)) \rangle_{\mathcal{N}(R(t), Q(t, t))}, \quad (4)$$

where

$$T(h) = 2T_p(h) - 1. \quad (5)$$

Closing the equation is trivial for binary neurons in the $x_i \in \{-1, 1\}$ Ising spin representation, because

their autocorrelation is always 1, so that $Q(t, t) = \frac{g^2}{N} \sum_i \langle x_i(t) x_i(t) \rangle = g^2$.

Rate model As a second model we consider continuous rate neurons with $x_i \in [-1, 1]$ and activation function $T: \mathbb{R} \rightarrow [-1, 1]$, timescale τ and a white noise process ξ . The relation between T and T_p is (5). There are two equivalent forms of the neuronal dynamics used in the literature, evolving according to

$$\tau \partial_t \mathbf{x} = -\mathbf{x} + T(\overbrace{\mathbf{J}\mathbf{x} + \sqrt{\tau}\boldsymbol{\eta}}^{\mathbf{h}}), \quad (6)$$

$$\Leftrightarrow \tau \partial_t \mathbf{h} = -\mathbf{h} + \mathbf{J}T(\mathbf{h}) + \sqrt{\tau}\boldsymbol{\xi}, \quad (7)$$

where, using the Greens function $L = (\tau\partial_t + 1)^{-1}$, the noise $\eta = L\xi$ is a low-pass filtered version of ξ . The latter is Gaussian and white $\langle \xi_i(t) \xi_j(s) \rangle = \sigma_\xi^2 \delta(t-s) \delta_{ij}$. These two equivalent forms have the significance that (6) is more descriptive of the 'rate neuron' dynamics, but (7) is more frequently used for calculations (e.g. Sompolinsky *et al.* [16], Schuecker *et al.* [26]) because the summation is outside of the nonlinearity. For the rate model (6), we write down the single neuron, single time slice of the full probability functional as $\rho[x(t)|h] = \delta[x(t) - \int_{-\infty}^t e^{-\frac{t-t'}{\tau}} T(h_i(t')) \frac{dt'}{\tau}]$, and take into account the noise term in $\rho[\mathbf{h}] = \delta[\mathbf{h} - \mathbf{J}\mathbf{x} - \sqrt{\tau}\boldsymbol{\eta}]$. Plugging into (3) we obtain the same equation (4) for the mean activity as for the binary neuron, if we choose the strength of the noise σ_ξ such that $Q(t, t) = g^2$ as well. The reason for the equivalence is that the exponential function appearing in the convolution equation is the Greens function L that we defined above. This proves that the binary and rate model with appropriate noise have equivalent mean activities and zero-lag autocorrelations in mean field approximation. The choice of the appropriate noise strength is discussed after we have extended the equivalence further in the next section.

B. Equivalent equations for time-lagged autocorrelations in binary and rate networks

While the similarity of $R(t)$ and $Q(t, t)$ is expected from the two model definitions, this is not so much so for the time-lagged autocorrelations $Q(t, s)$, the ingredient distinguishing dynamical mean field theory (DMFT) and mean field theory (MFT) in our use of language. For stationary rate neuron dynamics, $Q(\Delta t) := Q(t, t + \Delta t)$ follows as the solution of a Newtonian equation of motion [16, eq. 7]

$$\begin{aligned} \tau^2 \ddot{Q}(\Delta t) &= -V'_{R, Q(0)}(Q(\Delta t)), \\ V_{R, Q(0)}(Q) &:= -\frac{1}{2} Q^2 + g^2 \langle \mathcal{T}(h) \mathcal{T}(h') \rangle_{(h, h') \sim \mathcal{N}_{R, Q(0), Q}}, \end{aligned} \quad (8)$$

where $\mathcal{T}' = T$ and $\mathcal{N}_{R, Q(0), Q}$ is the bivariate Gaussian with stationary mean R and covariance matrix

$$\begin{pmatrix} Q(0) & Q \\ Q & Q(0) \end{pmatrix}.$$

To compute $Q(\Delta t)$ for binary neurons, we need more information about $\rho[x|h]$, namely the one neuron, two time slices joint probability distribution

$$\rho[x(t), x(s)|h] = \underbrace{\rho[x(t)|x(s), h]}_{\xrightarrow{t \rightsquigarrow s} \delta_{x(t), x(s)}} \rho[x(s)|h]. \quad (9)$$

To construct $\rho[x(t)|x(s), h]$ for binary neurons, the basic idea is to iterate the 2×2 states a neuron can assume at the points in time s and t and consider all its possibilities of evolution matching the respective initial and final condition. From such a consideration, we derive $Q(\Delta t) = Q(t, t+\Delta t)$ for stationary dynamics in App 2 by again taking a time derivative of the saddle point equation 3, yielding

$$\begin{aligned} \tau \frac{d}{d\Delta t} Q(\Delta t) + Q(\Delta t) \\ = g^2 \int_0^\infty \frac{dt'}{\tau} e^{-\frac{t'}{\tau}} \langle T(h) T(h') \rangle_{(h, h') \sim \mathcal{N}_{R, Q(0), Q(\Delta t+t')}}. \end{aligned} \quad (10)$$

This equation is the analogon of the integral equation (5.17) of van Vreeswijk and Sompolinsky [27]. The advantage of the form (10) is, as detailed in appendix App 2, that by differentiating once more with respect to Δt and then using Price's theorem [41], it can also be cast into the Newtonian form (8).

C. Mapping binary to rate networks with noise

Even though the differential equations for the time lagged autocorrelations are the same, their initial conditions are in general different in the two cases. Two initial conditions are needed for a solution. One is to require that $\lim_{t \rightarrow \infty} \dot{Q}(t) = 0$, which is the same in both cases. In the binary case, the second condition is $Q_b(0) = g^2$ because the zero-lag autocorrelation of a single spin is always one. In a rate network, however, the input noise strength determines how quickly the autocorrelation decays, resulting in the condition on the derivative $\dot{Q}_r(0+) = -\sigma_\xi^2/2$ Schuecker *et al.* [26] (note that our notational convention differs by the factor $1/2$). Here and in the following we use the subscripts b and r to refer to quantities of the binary and rate model, respectively.

The idea is now to choose an effective noise in the rate network such that $Q_r(0) = Q_b(0)$, so that not only the mean activities match, as discussed in Section II A, but also the time lagged solutions for the variance $Q(\Delta t)$.

To do so, using $\dot{Q}(\infty) = 0$ and conservation of total “energy” $V_{Q_0} + \tau^2 \dot{Q}^2/2$ implied by the Newtonian form of (8), the condition $Q_0 := Q_r(0) \stackrel{!}{=} Q_b(0) = g^2$ can be expressed as a condition for the derivative and thus the

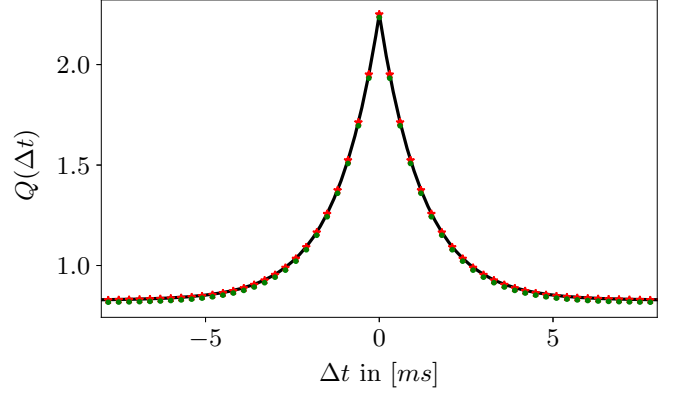


Figure 2. **Matched second order statistics in binary and rate networks.** Autocorrelation functions in simulations of binary (green dots) and rate networks (orange stars). Theoretical curve (black) given by solution of (8). Noise amplitude of the rate network chosen by (11) to obtain matched statistics. Other parameters: $N = 5000$, $g = 1.5$, $\bar{g} = 0$; simulation duration $T = 5000$ ms; autocorrelation averaged across all neurons.

noise amplitude

$$\begin{aligned} \frac{1}{2} \dot{Q}_0^2 + V_{Q_0}(Q_0) &= V_{Q_0}(Q_\infty)|_{Q_0=g^2} \\ \Rightarrow \sigma_\xi^2 &= 2 \sqrt{2(V_{g^2}(Q_\infty) - V_{g^2}(g^2))}. \end{aligned} \quad (11)$$

Therefore, given a pair of equivalent activation functions (5), moments of connectivity \bar{g} , g^2 , and timescale τ , asynchronously updated binary networks are statistically equivalent in DMFT approximation to rate networks with appropriately chosen Gaussian white noise input. This result is confirmed for $\bar{g} = 0$ in simulations by comparing the autocorrelation functions averaged across many neurons in (Figure 2). For $\bar{g} \neq 0$, we expect the same match, see also App 3.

Taking a step back, what is the intuition behind this result? When the binary neurons are averaged over realizations of the update time disorder, the Poisson update process with rate τ^{-1} becomes an exponential kernel corresponding to that of the rate network. The discrete jumps of the binary neurons around their mean become red noise, corresponding to the low-pass filtered noise η of the rate network (6). By nice conspiracy, this corresponds to simple white noise ξ in (7), which is also the version treated in most works on rate networks with noise, such as [18, 24, 26, 42–44]. This tight relation between binary and rate models is summarized conceptually in Figure 1b.

D. Binary networks are always chaotic in the thermodynamic limit

Given their statistical similarity, one may wonder if the network dynamics is identical in more respects. A partic-

ularly important measure for the computational ability of a network is its characterization in terms of chaoticity [13, 14, 16, 18, 26, 45].

So does the transition to chaos in rate networks [13, 16, 18, 26] translate to binary networks? We assess chaos by studying the time-evolution of the correlation between two systems with infinitesimally different initial conditions but identical connectivity in a replica calculation, an approach pioneered by Derrida and Pomeau [46]. We here do not use the classical annealed approximation, where the connectivity is redrawn in every time step, but compute the full quenched averages, where the connectivity is constant in time.

In appendix Section 4, by using an approach analogous to the derivation of the ODE for the autocorrelation (8), we obtain the equation governing the evolution of the cross-replica correlation

$$\begin{aligned} & \tau \frac{d}{dt} Q^{(12)}(t, t) \\ &= -Q^{(12)}(t, t) \\ &+ g^2 \left(1 - \langle |T(h^{(1)}(t)) - T(h^{(2)}(t))| \rangle_{h^{(1)}, h^{(2)}} \right). \end{aligned} \quad (12)$$

Here $(h^{(1)}, h^{(2)}) \sim \mathcal{N}(\mathbf{R}, \mathbf{Q})$ is a measure of a pair of Gaussian processes with mean $\langle h^{(\alpha)}(t) \rangle = R^{(\alpha)}(t)$, following (4) and covariance matrix $\langle h^{(\alpha)}(t) h^{(\beta)}(s) \rangle = Q^{(\alpha\beta)}(t, s)$, whose diagonal elements each obey (8).

Since the two replicas are nearly perfectly correlated in the beginning, we know that the correlation between a neuron and its 'copy' in the other replica is given by the autocorrelation at first, motivating the ansatz

$$Q^{(12)}(t) = Q_0 - \epsilon(t), \quad \epsilon(t) \geq 0.$$

As shown in appendix Section 4, an expansion for small ϵ leads to the approximate equation governing the evolution of $\epsilon(t)$

$$\tau \frac{d}{dt} \epsilon(t) = -\epsilon(t) + \frac{2}{\sqrt{\pi}} g^2 \langle T'(h) \rangle_{h \sim \mathcal{N}(R, Q_0)} \sqrt{\epsilon(t)}, \quad (13)$$

which generalizes the result of van Vreeswijk and Sompolinsky [27] to arbitrary activation functions. As was their classic conclusion, we see that independent of the parameters, the positive square root term is always larger than the negative linear term for small ϵ , so that the deviation will grow, indicating chaotic dynamics. Since the calculation becomes exact in the thermodynamic limit, the conclusion is that infinitely large binary networks are always chaotic, with formally infinite maximum Lyapunov exponent since the divergence is non-analytic. Since the slope of the activation function appears only averaged over the input distribution, there is no qualitative difference between different activation functions. In particular, going from a stochastic activation function to the deterministic Heaviside limit only changes the second term in (13) by a finite factor and thus does not qualitatively alter the chaotic behavior. This can also be

understood by noting that for the stochastic activation function, the function value at each update is compared to a random number to decide the activity state. This is just like using a Heaviside function but with randomly drawn threshold at each update.

Compared to a statistically matched rate-network, we find that the equation governing $\epsilon(t)$ is lacking a square root term for rate neurons [26, Appendix C]. Furthermore, in their chaos transition criterion [26, eq.20]

$$g^2 f_T(Q_0, Q_0) - Q_0 \geq 0$$

we see that when plugging in the matched statistics $Q_0 = g^2$ and using that $f_T \leq 1$, the condition for chaos is not fulfilled. The dynamics is therefore always in the regular regime because the frozen noise of amplitude given by (11) is large enough to drive the dynamics and to suppress chaos for $g^2 > 1$. Only asymptotically the chaos transition is approached for an infinite slope of the activation function, $T' \rightarrow \infty$, or equivalently $g^2 \rightarrow \infty$. This demonstrates a difference between the two models that is rooted in the effective noise: In the rate network, noise impinges from outside the network, and its realization is frozen in the replica calculation. In the binary network, noise is intrinsically generated by the discrete switching dynamics, so that the realization is not external and frozen, but depends acutely on the internal state.

There is an alternative intuitive way to interpret eq. (12): the change of the correlation is proportional to the mismatch between the correlation at time t , the first line on the right, and the correlation after being propagated once through the neuron model and connectivity, given by the second line. Thus the question of chaos can also be reinterpreted as a correlation transmission problem: Whether the two replicas will decorrelate or not depends on the way in which a correlation coefficient on the input side c_{in} is transmitted to the correlation of the outputs c_{out} which constitutes the future input correlation c'_{in} . Clearly, if $c_{\text{out}}(c_{\text{in}}) < c_{\text{in}}$, the correlation must decrease over time, and if $c_{\text{out}}(c_{\text{in}}) > c_{\text{in}}$, it regenerates.

The link to (12) can be made explicit by noting that the variance on the diagonal elements of \mathbf{Q} of the Gaussian measure $\mathcal{N}(\mathbf{R}, \mathbf{Q})$ are $Q^{(\alpha\alpha)} \equiv g^2$ and the covariance between replica is $Q^{(12)} =: g^2 c_{\text{in}}$, where c_{in} is the correlation coefficient between the input currents to the two neurons, each representing one replica. Defining the second line of (12) as $g^2 c_{\text{out}}$, one can interpret c_{out} as the correlation coefficient between the outputs of the two neurons (cf. Section 4, eq. (43)).

The transmission curve $c_{\text{out}}(c_{\text{in}})$ for discrete signaling is compared to the transmission curve for continuous signaling in Figure 3. While the slope $c'_{\text{out}}(c_{\text{in}} \rightarrow 1)$ for discrete signaling diverges as $\propto (1 - c_{\text{in}})^{-\frac{1}{2}}$, it stays finite for continuous signaling. The positive offset of the transmission curve for discrete signaling is a consequence of the random updating that is identical between the two neurons.

A consequence of the infinite slope c'_{out} is that an initial infinitesimal decorrelation grows infinitely quickly; the

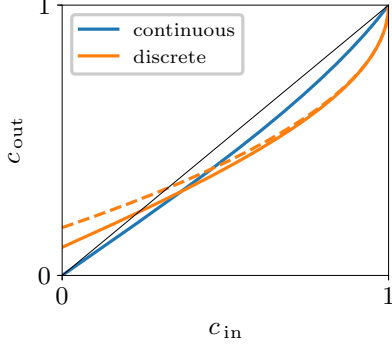


Figure 3. **Correlation transmission by a pair of neurons.** Correlation coefficient c_{out} between outputs as function of correlation coefficient c_{in} between inputs. Discrete signaling (orange, (52)); continuous signaling (blue, (49)). Approximation for discrete signaling in the limit $c_{\text{in}} \rightarrow 1$ (dashed orange) shows a behavior of the form $\propto -(1 - c_{\text{in}})^{\frac{1}{2}}$, so the slope diverges as $\propto (1 - c_{\text{in}})^{-\frac{1}{2}}$. For comparison: identity mapping with unit slope (black line).

Lyapunov exponent is infinite. The qualitative behavior of the correlation transmission curve for discrete signaling is the same for spiking models [47–52], explaining why these two model classes also behave similarly with regard to the transition to chaos. The underlying common reason is the discrete nature of the output variable: In both, the binary and the LIF model, the output of the neuron is binary, firing or non-firing. The divergence of the correlation transmission slope is a direct consequence of this discrete signaling; details are given in App 6.

For continuous-valued neuronal communication between neurons with activation functions that have finite slope, on the other hand, the transmission curve for correlations is always a function with a finite slope even for $c \rightarrow 1$. As a consequence, the chaos transition is qualitatively different; in particular, the Lyapunov exponent is finite here.

E. Transition to chaos in finite size binary networks

In contrast to the theoretical prediction, simulations of binary networks in fact show parameter regimes with regular dynamics. Since the theory is only exact in the limit of infinite network size, this suggests a finite size effect. But the result of the replica calculation (13) does not rely on carrying out the $N \rightarrow \infty$ limit, so it should still be a good approximation for finite, but large networks $N \gg 1$. Also the divergence of the correlation transmission slope is independent of N . How can the theory be reconciled with the simulation?

First, while the square root term in (13) is always larger for sufficiently small ϵ , there also exists a point $\partial_{\epsilon} \epsilon^* \stackrel{!}{=} 0$ where this relationship reverses and the linear

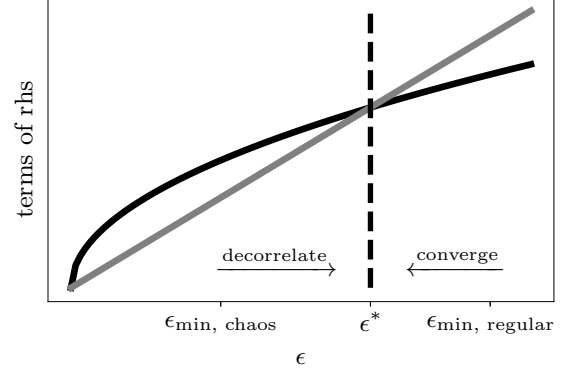


Figure 4. **Fixed-point average distance between replica implies chaotic-subspace.** The square root term $\propto \sqrt{\epsilon}$ (black curve) and the linear term $\propto \epsilon$ in (13) intersect and produce a fixed point ϵ^* for the covariance $Q_0 - \epsilon$ between the two replicas. The resulting average Hamming distance d^* between states in the two copies of the system is given by ϵ^* and (16) as $d^* = N\epsilon^*/g^2$. Depending on whether ϵ_{min} (which corresponds to a Hamming distance of $d_{\text{min}} = 1$) is smaller or larger than ϵ^* , the replicas will either decorrelate, or they will converge and forget the perturbation.

term starts to dominate: The point where the right hand side of (13) vanishes,

$$\sqrt{\epsilon^*} = \frac{2}{\sqrt{\pi}} g^2 \langle T'(h) \rangle_h. \quad (14)$$

This point corresponds to a stable average distance between (partly) decorrelated trajectories, as illustrated in Figure 4. This point can be interpreted as the intersection of the correlation transmission curve with the identity line in Figure 3: The curve for discrete signaling shows a stable fixed point at nonzero correlation, while that for the continuous case does not.

Second, in a finite network of N binary neurons an infinitesimal perturbation cannot be realized, since the smallest possible perturbation is to flip a single spin. This would mean a perturbation in the other neurons' input by Δh_{min} , which is distributed as $\rho(\Delta h_{\text{min}}) = \mathcal{N}\left(2\frac{\bar{g}}{N}, 4\frac{\bar{g}^2}{N}\right)$ due to the connectivity. Using the general relation $\langle \Delta h^2 \rangle = 2\epsilon(t)$ we obtain an average minimal decorrelation

$$\epsilon_{\text{min}} = \frac{1}{2} \langle \Delta h^2 \rangle_{\rho(\Delta h_{\text{min}})} = 2\frac{\bar{g}^2}{N} + \mathcal{O}\left(\frac{\bar{g}^2}{N^2}\right).$$

Therefore, if $\epsilon_{\text{min}} > \epsilon^*$ the replica will tend towards more correlation. But as the only possible step below ϵ_{min} is having zero different spins and thus perfect correlation, the initial difference should tend to be completely forgotten, resulting in regular dynamics. On the other hand, if $\epsilon_{\text{min}} < \epsilon^*$ an increase of the initial difference is possible.

Thus the chaos transition criterion in the finite binary

network is $\epsilon_{\min} \stackrel{!}{=} \epsilon^*$ resulting in

$$1 \leq \sqrt{\frac{2}{\pi}} g \langle T'(h) \rangle_h \sqrt{N}. \quad (15)$$

The predicted transition and also the residual correlation ϵ^* fits that observed in simulations quite well (Figure 5).

Due to the scaling with \sqrt{N} , it is clear that networks with thousands or even only hundreds of neurons are only non-chaotic if the connectivity is very weak or the dynamics saturated (which gives a small $\langle T'(H) \rangle_H$). Also, $N \rightarrow \infty$ clearly recovers the limit of strictly chaotic dynamics. For the special case of a Heaviside activation function and vanishing mean connectivity $\bar{g} = 0$, the network is always chaotic, since $\langle H'(h) \rangle_{h \sim \mathcal{N}(0, g^2)} = \sqrt{2/(\pi g^2)}$ results in $\pi/2 \leq \sqrt{N}$, which is certainly true for typical network sizes.

We also obtained the same criterion (15) via a less general, but more intuitive perspective by analyzing the probability that, given a single spin difference, the difference in inputs is such that during the next updates, another neuron will also be updated to a 'wrong' state (see App 5). This view provides an expression for the average rate of decorrelation steps caused by an initial decorrelation step. Requiring this rate being unity, we obtain the same chaos transition criterion as (15). The approach is inspired from and very similar to calculating the divergence rate of fluxtubes in spiking networks [53]. Indeed, the binary network has relatively trivial fluxtubes in their input phase-space given by those regions that result in the same updated state.

F. Computation in chaotic binary networks is governed by a chaotic sub-manifold

The general behavior of the network is that nearby trajectories diverge at first but do not decorrelate completely. Instead, any pair of trajectories has an average maximal distance determined by ϵ^* . This reflects that the two trajectories are evolved by the same network connectivity and update sequence. Also trajectories that are very far apart will converge to this residual correlation. The fixed-point distance ϵ^* is thus a representative of the average distance between any two trajectories in the long time limit. The corresponding Hamming distance $H_{12} = \frac{1}{4} \|\mathbf{x}^{(1)} - \mathbf{x}^{(2)}\|^2$, that is the number of different spins between a pair of binary states, is given by

$$\begin{aligned} Q_{12}(t) &= \underbrace{Q_0}_{g^2} - \epsilon(t) = \frac{g^2}{N} \sum_j \langle x_j^1(t) x_j^2(t) \rangle \\ &= \frac{g^2}{N} (N - 2H_{12}(t)) \\ \Rightarrow H_{12}(t) &= \frac{N \epsilon(t)}{2g^2} \end{aligned} \quad (16)$$

where the pre-factor of H_{12} arises because every flipped spin causes a decrease by 2 (from +1 to -1). Even though

the H_{12} spin flips distinguishing two trajectories can in principle be distributed across any of the N neurons, the subspace spanned by the set of possible trajectories has an approximate dimensionality of $d(t) \simeq 2H_{12}(t)$. This can be understood by considering the first two lines of (16): a distance of H_{12} has the same effect on the sum of correlations as a number of $2H_{12}$ uncorrelated spins would have. Stated differently, the Hamming distance H_{12} is the same as the average distance of d putatively independent spins that take the values $\{-1, 1\}$ with equal probabilities.

Thus, if $\epsilon_{\min} > \epsilon^*$, then $d(\infty) < 1$ and the set of long term trajectories contains only a single trajectory (fluxtube), thus constituting a limit cycle (although the return time is astronomically large [54]). Irrespective of the initial state, the network is attracted to a stereotypical trajectory. This situation arises for very weak coupling. Obviously, such a network is weak in performing computations, because different inputs lead to the same final state within short time.

If $\epsilon_{\min} < \epsilon^*$, then $d(\infty) > 1$ and there are many trajectories (fluxtubes) that constitute the attractive subspace. The evolution within the space is chaotic, because for any pair of states with an initial distance $\epsilon < \epsilon^*$ the distance increases; thus small differences are amplified. This is visible in the raster plots in Figure 6a: Short after stimulus onset, network states are quite similar across stimuli. As time progresses, the number of neurons in different states grows, as indicated by their distance (Figure 6b). An initially low-dimensional set of stimuli is thus expanded into a higher dimensional representation. For long times, however, the two states differ in only typically $d(\infty)/2$ of their neurons. This limiting dimensionality grows proportional to Ng^2 as seen by inserting (14) into (16)

$$d^* = g^2 N \left(\frac{2}{\sqrt{\pi}} \langle T'(h) \rangle_h \right)^2. \quad (17)$$

Variability across different stimuli is thus intimately related to the dimensionality of the binary networks activity. From the viewpoint of computation, the number of fluxtubes in the attractor gives a measure of the number of distinguishable states in the networks memory.

What are the consequences for computation by discrete-state networks?

To address this question, we investigate the network in a setting of reservoir computing, trained to classify P random binary patterns: A subset of size L of the N neurons is prepared in an initial state at $t = 0$. This initial state represents one of P different input patterns to the network; we number patterns by index α . At each time t , we train a linear readout $S_\alpha(t) = w_\alpha(t)^T x_\alpha(t)$ by linear regression to provide the output $S_\alpha(t) = 1$ if the α -th pattern has been presented and 0 else (see App 7 a). Thus we have P readouts, one for detecting each of the presented patterns. While training and testing, we use noisy realizations of the patterns by applying an additional Gaussian independent noise of variance σ^2 to each entry of a pattern.

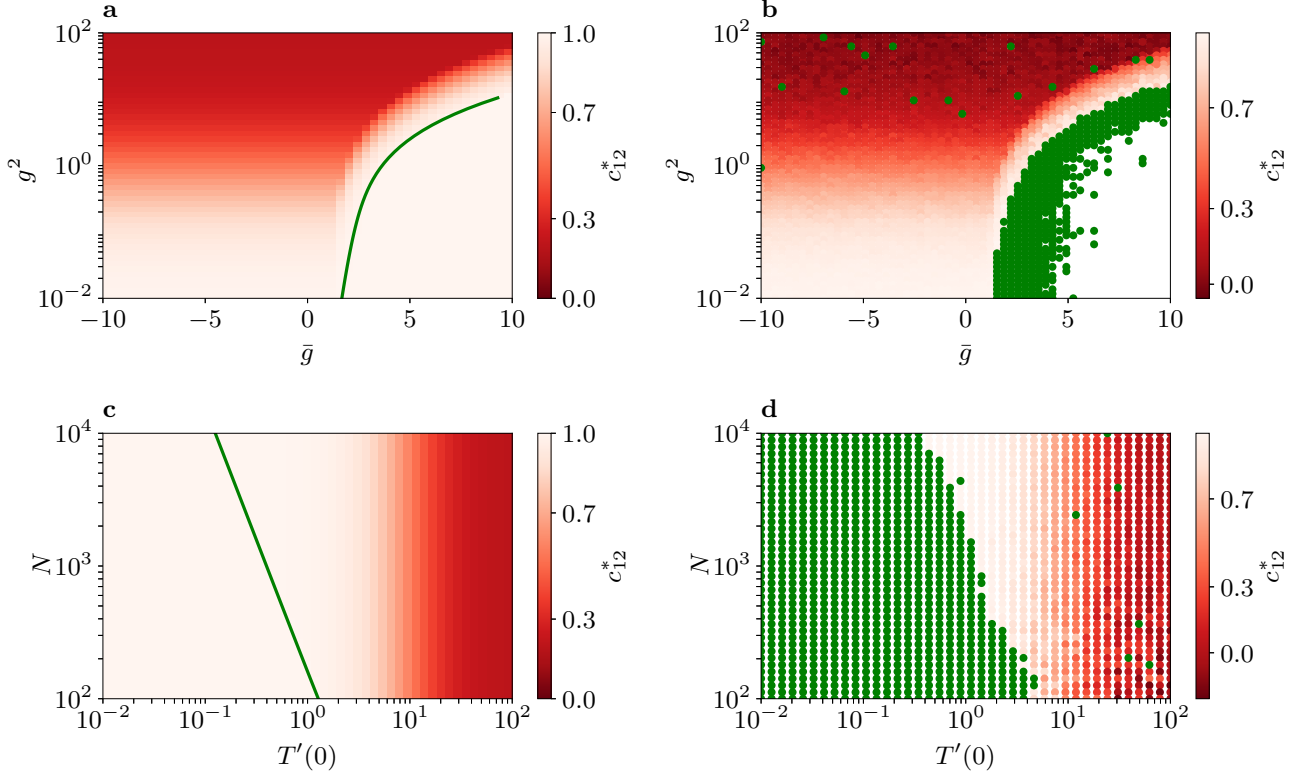


Figure 5. **Chaos transition and residual correlation in theory (a,c) and simulations (b,d).** **a** Theoretical prediction of chaos transition (green line, eq. (15)) and residual correlation coefficient between replicas (red shading, $c_{12}^* = 1 - Q_0^{-1}\epsilon^*$ and eq. (14)) for varying mean \bar{g} and variance g^2 of the connectivity. Other parameters are $N = 5000$, $T = \tanh$, $\tau = 10$ ms. **b** As in (a) but each pixel is colored red (chaotic) or green (stable) according to a network simulation. Two identical networks were evolved with identical random numbers, only one being perturbed by flipping two spins, and after $T_{\text{sim}} = 2500$ ms the correlation between the state vectors was computed. The few scattered green dots in the chaotic regime are algorithmic artifacts where the perturbation was unsuccessful. **c** Theoretical prediction for varying network size N and slope of the activation function $T(h) = \tanh(T'(0)h)$. Note that the predicted residual correlation is independent of N (compare (14)), while the chaos transition depends on N (compare (15)). Other parameters are $\bar{g} = 0$, $g^2 = 0.01$ and $\tau = 10$ ms. **d** As in (c) but from network simulations. Simulations done as described for (b). Note that the chaos transition in simulations happens slightly later than predicted by (15). This could be anticipated, since if the average proliferation rate of flips per time constant is only slightly above one, the cascade triggered by the perturbation still has a large probability of dying out.

The dimension $d_s(t)$ of the subspace spanned by presenting different patterns α is rapidly increasing with time and then converges to the residual value predicted by numerically integrating (13), as shown in Figure 6b. This transient dimensionality increase improves the linear separability of the patterns, causing the signal read-out to increase, shown in Figure 6c. This can be understood from the property of the linear regression; if network responses were pairwise orthogonal, which is to good approximation satisfied in the high dimensional signal subspace, the signal would be

$$S_\alpha(t) = \frac{d_s(t)}{P}$$

as shown in App 7b.

However, also the distance d_n between two noisy realizations of the same pattern increases. But d_s has a

head start because noise realizations are more similar to each other than to other patterns. Now let us assume that different noise realizations cause different responses that lie entirely within the subspace of the signal. This means that the noise flips a number of spins and thus effectively reduces the dimensionality of the space that faithfully encodes the signal. The effective dimension of the space that is available to represent the signal is then

$$d_{\text{eff}} = d_s - d_n,$$

where d_n is the dimensionality of the space spanned by different noise realizations. The expected signal is then

$$\begin{aligned} S_{\alpha'}(t) &= \frac{d_s(t) - d_n(t)}{P} \\ &= \frac{d_s(t)}{P} \left(1 - \frac{d_n(t)}{d_s(t)} \right). \end{aligned} \quad (18)$$

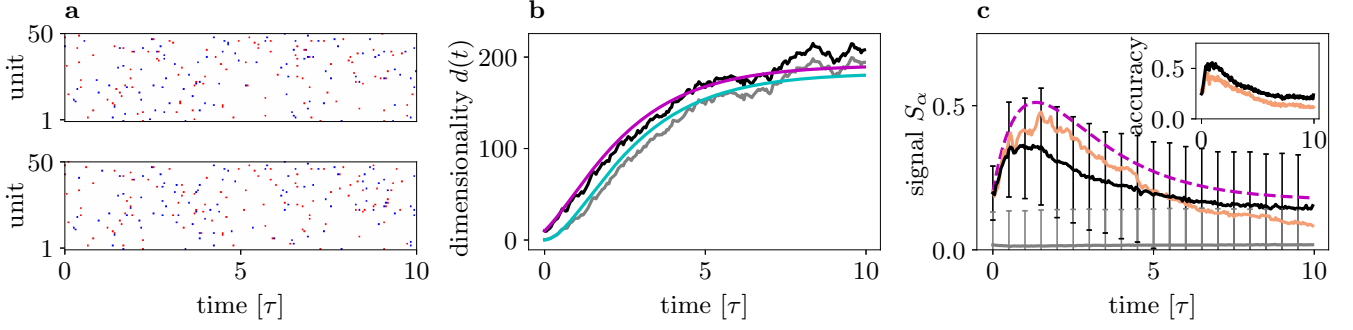


Figure 6. **Transient dimensionality expansion of stimulus representation by a chaotic binary network.** **a** Time evolution of first 50 neurons for two different initial stimulus patterns; up transitions in red, down in blue. Stimulus applied by initializing first $L = 10$ neurons to one of the $P = 50$ fixed, random patterns; individual neurons in each pattern take the states $\{-1, 1\}$ randomly with equal probability. **b** Dimensionality $d_s(t)$ explored by the network across different stimuli (black; theory (13) in magenta). Dimensionality $d_n(t)$ due to different noise realizations of a pattern (gray; theory (13) in cyan): Gaussian noise with standard deviation $\sigma = 0.3$ added to each of the L entries of the initial pattern state. **c** Linear readout $S_{\alpha'}(t) = w_{\alpha'}(t)^T(x_{\alpha}(t) + \xi_{\text{pre}}) + \xi_{\text{post}}$ trained for each time point t to detect stimulus identity by minimizing quadratic error $\sum_{\alpha} (S_{\alpha'} - \delta_{\alpha\alpha'})^2$ for matching the stimulus $\alpha = \alpha'$ (black) and non-matching stimuli $\alpha \neq \alpha'$ (gray). Error bars show the variability across patterns and noise realizations. Theoretical prediction (18) in dashed magenta. Readout using the approximated weight vector (55) that assumes an orthogonal representation (orange). Inset: classification accuracy of the initial input stimulus based on choosing the readout with largest signal. Note that the approximate readout vectors yield a higher average signal, but also the variance is higher (not shown) resulting in slightly worse classification accuracy. Other parameters: $N = 500$ neurons, coupling strength $g = 0.8$, pre-readout noise $\sigma_{\xi, \text{pre}} = 0.1$ and post-readout noise $\sigma_{\xi, \text{post}} = 0.1$ as detailed in 7. The training set comprised 100 noisy realizations of each pattern, and the test set 20.

The latter form explains qualitatively the shape of the signal shown in Figure 6d: Initially, the signal rises in relation to the ratio of dimension of representation space and number of patterns, but ultimately, the signal declines, because the dimensionality spanned by the noise approaches that spanned by the signal. This transient dimensionality expansion happens very fast: Using that (15) gives the average number of flips n_{spawns} caused by an initial flip within one time constant (as obtained in App 5), we note that

$$\frac{d^*}{2} = n_{\text{spawns}}^2,$$

so that the decorrelation always happens on the timescale of two time constants, independently of all parameters.

Note that neither in theory nor in the simulation the average signal drops to zero for $t \rightarrow \infty$; this is because not all noise realizations leave the fluxtube of the original pattern, so that the average distance between realizations remains smaller than that between patterns (analyzed in App 7c).

G. Difference and similarity to transient signal amplification in the rate model

If the same task is performed by a network of rate units with matched statistics, the performance is close to zero. This is because the matched rate models are always in the non-chaotic regime as chaos is suppressed by the effective noise (as noted in Section IID), so that trajectories for different presented patterns converge. Any tiny

readout noise destroys classification accuracy, as shown in Figure 8a.

However, how does computation in the chaotic regimes of binary and rate nets compare? For this we give up the match of statistics between the binary and rate models and from here on consider a rate network without effective noise and $g^2 > 1$.

Using a replica calculation in dynamical mean field approximation, the equation governing the evolution of the cross-replica time-lagged covariance in the rate model is of the form [18, 26]

$$(\partial_t + 1)(\partial_s + 1)Q^{(12)}(t, s) = g^2 f_T(Q_0, Q^{(12)}), \quad (19)$$

with $f_T(Q_0, Q^{(12)}) = \langle T(x_1)T(x_2) \rangle$ and the average is taken with regard to $(x_1, x_2) \sim \mathcal{N}\left(0, \begin{pmatrix} Q_0 & Q^{(12)} \\ Q^{(12)} & Q_0 \end{pmatrix}\right)$.

The approximation for small differences $Q^{(12)} = Q_0 - \epsilon$ to linear order in ϵ is

$$(\partial_t + 1)(\partial_s + 1)\epsilon(t, s) = g^2 f_T(t, s)\epsilon(t, s). \quad (20)$$

Since there is no term $\propto \sqrt{\epsilon}$, there is no residual correlation for small ϵ . Furthermore, in the equation (19) valid also for ϵ large, the completely decorrelated state $Q^{(12)} = 0$ is always a fixed point because then the expectation value factorizes, and by the point symmetry of T the right hand side vanishes. In the thermodynamic limit, the residual correlation in rate networks is thus zero for any $g > 1$. Indeed, trajectories in large rate networks show very small residual correlation already directly beyond the edge of chaos $g^2 \gtrsim 1$, as shown in Figure 7c (inset).

However, as already noted by Sompolinsky *et al.* [16], the transition at $g = 1$ is not completely sharp for smaller networks, which must be a finite size effect not included in the employed mean-field approximation. We here observe the same effect, that small rate networks show a residual correlation between trajectories, shown in Figure 7c. For larger networks, however, the residual correlation approaches zero; this is a qualitative difference to binary networks, which can have a finite residual correlation (17) also in the large N limit.

As shown in Figure 7b, also finite chaotic rate networks show a transiently smaller difference between noisy realizations of a pattern than between patterns in the classification task. This also follows from (20) since the acceleration of the decorrelation is smaller for smaller initial ϵ , making the noise distance grow slower than the signal distance. The finite rate and binary networks therefore can both have a residual correlation and a transient difference between signal and noise amplification, although the effects are controlled differently by the parameters.

Another difference is seen in the timescale of decorrelation in Figure 7b: In the rate network it takes many neuronal time constants; this time only gradually shortens by increasing g . In the binary network decorrelation is always fast, taking a few neuronal time constants at most. This can be understood in terms of the decay constant of the time lagged autocorrelations: In a noiseless rate network, the autocorrelation decay constant diverges at the transition to chaos. In the binary network, however, the effective noise of the discrete dynamics causes a smaller, finite decay constant and there is also no qualitative difference between the autocorrelation shape in the regular and in the chaotic regime. Indeed, as we have shown in Section II F, their decorrelation always takes on the order of two time constants, largely independent of g .

The next difference becomes apparent when considering the classification performance of the rate network. As shown in Figure 8b, the accuracy jumps to a high value after the first time step, instead of gradually increasing within approximately one time constant as in the binary network. How can this behavior be understood? The reason is that in the rate network, all neuron states are immediately and also nonlinearly affected by the input pattern, so that it is immediately projected nonlinearly into a N -dimensional representation that allows linear classification. This becomes apparent by considering that in the time step after stimulus presentation, the input to the network contains a term $\propto \frac{\delta t}{\tau} \sum_j J_{ij} T(h_j(0))$ which performs a non-linear embedding of the stimulus into the N -dimensional space.

Of course, even though the dimensionality is immediately N -dimensional, the amplitudes must grow continuously and are very small at first. This also highlights a difference in the interpretations of ϵ : In the binary network, there is a direct link between ϵ and the dimensionality of the signal space, while in the rate network ϵ

is just a measure of the distance between trajectories and is only very indirectly related to the number of dimensions across which this distance is distributed. Hence the peak of the difference between inter- and intra-pattern distances in Figure 7b does not correspond to a peak in classification accuracy in Figure 8b, since it describes a transient signal amplification, and not also a transient dimensionality expansion as in the binary network case.

Still, even though the dimensionality of the representation already initially equals N , distances between stimuli are at first small. The classification in the rate network therefore relies on fine-tuned and very large readout weights in the beginning Figure 8d. Therefore, the initial classification accuracy is severely affected by adding weak noise to the readout (Figure 8c). This, in turn, results in a peak of the accuracy predictable by the theoretical peak in signal amplification (Figure 7a). In summary, the main differences between the chaotic behavior of binary and rate networks are the decorrelation time scales, behavior of the residual correlation, and the location of the chaos transition.

III. DISCUSSION

Overall, our analysis shows that networks of units coupled by continuous signals and those communicating by discrete signals are very closely linked on the level of their activity statistics. Concretely, we show that by adding appropriate noise, a network of continuous rate neurons can be matched to the same network of binary neurons, having exactly the same dynamic mean-field theory. This is because the binary network has the same mean activity but additional discretization noise.

Qualitative differences, however, arise for their information processing capabilities: We find a generic mechanism that creates an attractive chaotic sub-manifold in networks with discrete signaling whose dimensionality is a finite fraction of the network size. This mechanism fosters a transient expansion of applied signals within few neuronal time constants into a progressively higher dimensional space, enabling such networks to display augmented signal separability with high noise tolerance. However, a rate network that is matched to the statistics of a binary network is never in the chaotic regime and thus does not display this computational ability. Moreover, there is no such subspace that can be identified in continuously coupled networks. We discuss the implications and the limitations of the statistical match between the two model classes in Section III A, and discussion of the chaos and computation aspects follows in the sections Section III B to Section III D. Section III E takes a step back and reflects on possible consequences of these insights for information processing in the brain.

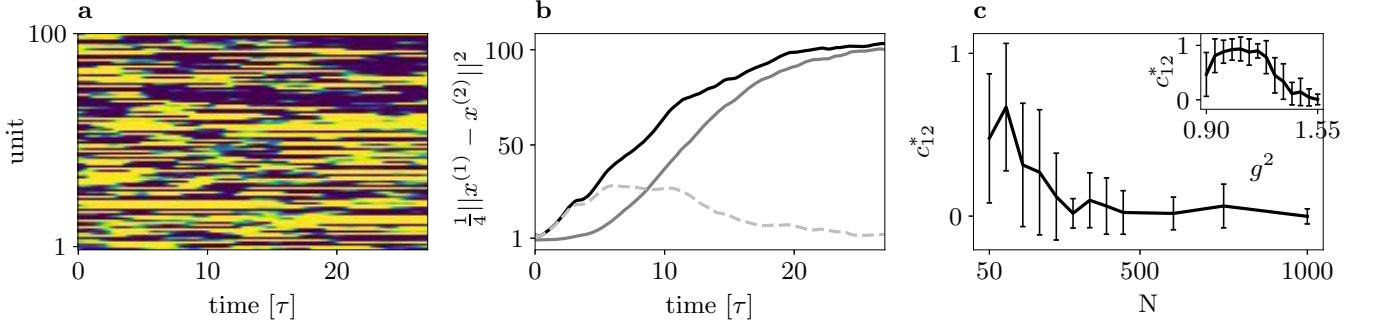


Figure 7. **Evolution of trajectories in a chaotic rate network.** **a** Chaotic network activity for $N = 250$, $g = 5.8$, $\sigma_{\text{eff}}^2 = 0$ and $T(h) = \tanh(h)$. **b** Time evolution of average distances between patterns (black) and between noisy realizations of a pattern (midgray). Difference between signal and noise distances (gray, dashed). Network as in (a) and $P = 50$, $L = 10$, $\sigma = 0.3$. **c** Strong dependence of the residual correlation c_{12}^* on network size (x-axis) and connectivity realization (error bars), for $g = 2$. Inset: fast decay of residual correlation at the edge of chaos for $N = 1500$.

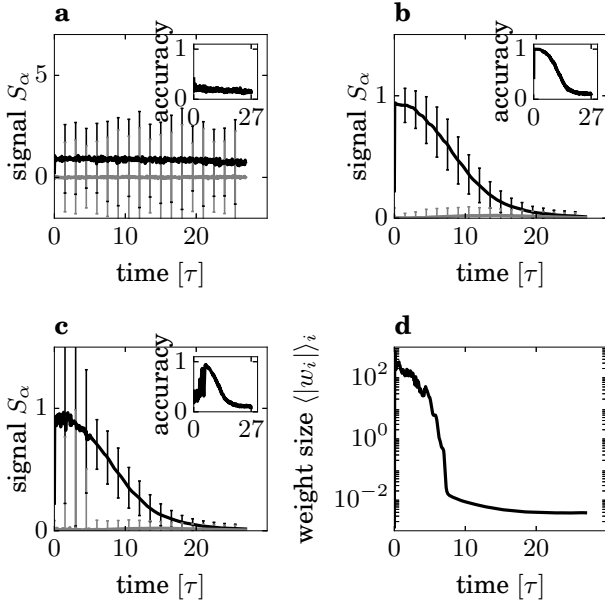


Figure 8. **Stimulus representation in a rate network.** **a, b, c** Signal of correct readout (black), signal of wrong readouts (gray), and classification accuracy (inset). **a** Including noise σ_ξ^2 matched to the statistics of a binary network according to (11). Parameters otherwise as in Figure 7. Because the frozen effective noise suppresses chaos, trajectories for different stimuli converge towards the same state and a small readout noise $\sigma_{\text{readout}} = 10^{-4}$ results in classification at chance level. **b** Removing the noise in the network, and no readout noise. The network is chaotic as in Figure 7, and classification accuracy jumps to 1 in the first time step. **c** Including readout noise $\sigma_{\text{readout}} = 10^{-4}$ impedes classification accuracy until trajectories are sufficiently separated. **d** Average norm of individual readout weights for the setting in (b). Since trajectories are very close in the initial time period (compare also Figure 7b), initial readout weights are very large, explaining the sensitivity to readout noise in (c).

A. Correspondence of statistics in binary and rate networks

In general, it is not known on which level biological neuronal networks should be modeled in order to understand their function. Therefore, approaches on all kinds of levels exist, but the problem of choosing an appropriate level largely remains. Exposing identities and differences between neuron models is thus necessary, since the generalization of results across different models is otherwise unclear. In particular, we here asked the question: Does it matter if we use continuous or discrete signaling? This question is here addressed by comparing binary and rate networks. Steps in this direction were already taken in Grytskyy *et al.* [55], who showed a mapping of leaky-integrate-and-fire (LIF) neurons, Hawkes processes, and binary neurons to noisy linear rate models. The results presented here are in line with their results on binary and linear rate neurons, but more general since they apply not only to the linearization of the models but hold for the nonlinear behavior as well. As our work aims at a unified picture of neural network models, we derived a model-independent field theory approach that provides an ideal tool for such an investigation. We have not focused on a technical study of this path integral formulation here, which will be subject of a forthcoming manuscript. Applied to the binary and rate network models, we exposed a one-to-one match of their activity statistics in dynamical mean field approximation. Only this statistical equivalence enables us to contrast their dynamical and computation properties in a comparable dynamical state.

We now give a technical discussion concerning assumptions and expected generalizability of the statistical mapping.

Single population with random Gaussian connectivity.

The assumption of Gaussian connectivity $J_{ij} \sim \mathcal{N}(\frac{g}{N}, \frac{g^2}{N})$ simplifies the equations and the derivation of the DMFT. The results straight-forwardly generalize to multiple populations, as the equations acquire population indices but

stay structurally the same. Multiple populations were treated for binary neurons [27] and for rate neurons [18, 43]. We scaled the mean connectivity as \bar{g}/N to obtain a consistent approximation in orders of $1/N$ when applying the saddle-point approximation to the auxiliary fields. Thinking in orders of $1/N$, using \bar{g}/\sqrt{N} instead would make it necessary to include also Gaussian fluctuations of the mean activity field $\langle \mathcal{R}^2 \rangle \sim 1/N$, corresponding to linear response theory. However, contributions of such fluctuation corrections are small in the inhibition dominated regime $\bar{g} < 0$ where fluctuations are suppressed by negative feedback [56]. The results also generalize to non-Gaussian synaptic weight distributions, as long as higher than second cumulants are suppressed by powers of N^{-1} , such as for sparse connectivity. This is because only the first two cumulants of the connectivity enter in dynamical mean field approximation. Scale-free distributions of weights can violate this assumption and require a different approach [57].

Other extensions If one were to match the statistics on the single neuron level instead, each neuron would need an individual noise strength dependent on its mean activity.

Matching the models for non-stationary trajectories would require a time-dependent analysis of the mean field equations.

Asynchronous update. Since asynchronous updating models the membrane time constant and irregular spiking of neurons, we prefer it as a neuron model. Synchronous updating is analytically slightly simpler and also frequently used, for example by Bertschinger and Natschläger [14], but replaces the intrinsic time scale τ by the ‘time’ between updates. While the zero time-lag stationary statistics are the same [58], the time lagged autocorrelations differ and dynamical differences may appear at the timescale of single updates, relevant for the computational properties in section Section II F. Especially, we expect that for synchronous updating, the residual correlation is smaller, behaving more like that in a rate network, because the correlating effect of using the same update sequence in both replicas is missing.

Same activation function, time scale, connectivity and dynamic range. Activation function and time scale must be the same in both models, but the connectivity only has to be drawn from the same distribution, since the statistics is matched on the population level only. As the dynamic ranges we used $x_b \in \{-1, 1\}$ and $x_r \in [-1, 1]$. In general, other finite ranges like $[0, 1]$ do not change the result as long as they are the same in both models. An unbounded range would make no sense for the binary neurons with two activity levels. This point is connected to the interpretation of a binary neuron’s active state as that for an average time τ it is firing at its maximal rate, not that it fires a single spike. This must be so since it can only be active with a rate τ^{-1} but the saturated firing rate of the modeled neuron may be higher. Therefore, if one would like to interpret activations of binary neurons as binned Poissonian spike trains,

activity must be sparse enough to have a low probability of two spikes falling in the same time bin. The binning width τ cannot be changed for binary neurons since it models the membrane time constant by ensuring that an activation’s probabilistic effect on its synaptic partners declines exponentially on scale τ . Then the lower range of the activation function can be interpreted as modeling a spiking neuron’s transfer function for low firing rates.

Approximation of inputs as independent Gaussian processes. The formal saddle point approximation in the auxiliary fields \mathcal{R} and \mathcal{Q} implies a Gaussian approximation of the input currents $h_i \stackrel{\text{i.i.d.}}{\sim} \mathcal{N}(\mathcal{R}, \mathcal{Q})$. Therefore, we have neglected cross correlations between neurons. They can be incorporated by computing fluctuations of the auxiliary field \mathcal{R} ; they are the same in both models, as they are driven by the autocorrelations and follow from linear response theory [55, 59]. The field theoretical approach gives a systematic framework to compute not only those correlations, but in principle also arbitrary higher-order fluctuation corrections. Going beyond Gaussian fluctuations would mean that the noise that needs to be added to the rate network may in general also get colored or non-Gaussian corrections.

B. Difference of dynamics between the models

Concerning the question in how far known results on chaos in rate networks translate to the behavior of binary or spiking networks [17, 19–22], we demonstrate that the dynamical state in binary and rate nets is qualitatively different even if they are statistically equivalent. While infinitely large binary nets are always chaotic, as shown for the special case of Heaviside activation functions in the classical paper by van Vreeswijk and Sompolinsky [27], rate networks with matched statistics are not chaotic, since the effective noise, which increases with increasing connectivity strength, is strong enough to suppress chaos [26]. Only in the limit of an activation function with infinite slope (or alternatively $g^2 \rightarrow \infty$) also the rate net is chaotic, which is consistent with Kadmon and Sompolinsky [18]. This result also relates to the observation that when linearizing a binary network around its working point, the effective spectral radius is always smaller than unity [60].

Our explanation for the difference is that in the rate network, the noise used is external and frozen, but a binary network’s noise realization depends acutely on the initial value of the system. Thus, perturbing the initial value also changes the noise realization. Especially, due to the discrete signal conveyed to receiving neurons, a microscopic perturbation that flips the state of a single neuron can cause a macroscopic change of the network state; the probability that this happens increases with the number of targets that receive this perturbation, thus with network size; this is due to the strong synapses $J_{ij} \propto N^{-\frac{1}{2}}$. For large networks the growth of the perturbation corresponds to a macroscopic change in

the noise realization.

Another, complementary explanation arises from the replica calculation. As we have shown here, this method reduces the question of a chaos transition to the study how correlations are transferred from the inputs to a pair of neurons to their outputs. In particular, one needs to consider how the correlation between outputs declines as the correlation of their inputs falls below perfect correlation $c \lesssim 1$. We have shown here that neurons with discrete signaling necessarily show a diverging correlation transmission slope at the point of perfect correlation between their Gaussian-distributed inputs. Therefore networks of such neurons have an infinite Lyapunov exponent for $N \rightarrow \infty$. For continuous signaling, the slope is always finite as long as the slope of the activation function is bounded, resulting in finite Lyapunov exponents.

This connection between correlation transmission of a neuron model and chaotic dynamics of their networks also opens possibilities of future work, since the correlation transmission of neurons is well studied experimentally and theoretically [50, 51, 61, 62, e.g.]. Especially, the diverging behavior of the correlation transmission slope of binary neurons is also seen for spiking neurons without reset [51] and for the LIF model [48–50, 52, 63], suggesting that these model classes behave similarly with regard to the transition to chaos.

C. Chaos and flux tubes in finite binary networks

We have demonstrated that there is a transition to chaos transition in finite-size binary networks that is accessible to a field theoretical replica calculation. Our results are in line with older works showing a chaos transition in random boolean networks for indegree $K = 2$ [46, 64], which relates to the transition at $N \approx 2$ for the Heaviside activation function. Derrida and Pomeau [46] used the annealed approximation, while we computed fully quenched averages over the disorder. The results are supported by simulations.

Moreover, we here demonstrate a tight link between the replica calculation and the treatment of chaos in spiking networks in terms of the divergence rate between flux tubes [23]. In spiking networks, the flux tube boundaries in phase space are given by deviations that cause a change in the global spike order at some point in the future [53]. The situation is exactly the same in a binary network, where changes in the activation pattern are investigated instead of spike patterns. But binary neurons are formally simpler, as there is no internal state like the membrane potential and the activation times cannot vary continuously but are constrained to the predetermined update times. Therefore perturbations inside a flux tube are not forgotten exponentially as in LIF neurons but instantly. Just like in LIF networks, the effective distance to a boundary shrinks with network size as $\sim 1/N$. The divergence rate between flux tubes scales as $\sim \sqrt{N}$, opposed to $\sim N$ in the LIF network [23]. Both are

clearly consistent with an infinite Lyapunov exponent for $N \rightarrow \infty$.

D. Computation in large networks with discrete signaling

We have shown that the activity of chaotic binary networks is governed by an attractive chaotic sub-space which does not exist in this form in rate networks: in binary networks its dimension is a finite fraction of the number of neurons, while in rate networks the entire space forms the chaotic manifold. Also the transition to chaos is caused by different mechanisms and occurs at different points in parameter space. Therefore, we argue that computation at the edge of chaos in networks with continuous and discrete signaling is behaving qualitatively different, which is in line with the work of BÜsing *et al.* [19]. We were able to expose these differences as originating solely in the difference of signaling by using otherwise equivalent models and treating them in a unified framework.

Our analysis of the reservoir computing inspired classification paradigm shows mechanistically how the transient dimensionality expansion of the noisy signal first increases the performance, until entropy production catches up and the representation is too much corrupted by the amplified noise, preventing linear classification.

What is the connection to previous works on the relation of chaos and computational power? It has often been argued that close to the edge of chaos, networks show an optimal trade-off between separation of stimuli and generalization across stimuli [13, 14, 45, 65]. Our analysis of transient dimensionality expansion in binary networks and transient signal expansion in rate networks provides a time resolved perspective to this picture. Indeed, the signal and noise dimensionalities that we analyzed as approximate measures controlling the classification performance, can be compared to the Kernel Quality and Generalization Rank (VC-dimension [66]) measures introduced by Legenstein and Maass [65]. Our results furthermore show that for binary networks, the memory lifetime is never very long, but different than in rate networks, it also does not strongly reduce when moving deeper into the chaotic regime. Therefore, while not being suitable for tasks that require long memory, performance may benefit from an increasing separation ability even deep in the chaotic regime, because with increasing network size also the peak of the informative dimensionality $\max(d_s - d_n)$ continues to rise. This can also be seen in the results of Snyder *et al.* [67], where for small readout delay, performance stays high for larger indegrees (e.g. their fig3 a,b). Overall, this raises the question, whether this effect could be combined with a longer memory lifetime, for example by using neurons or synapses with heterogeneous intrinsic time constants, adding clustered connectivity, or feeding the readouts back into the network. We will investigate this in future work.

As the peak performance is reached on the scale of a single neuronal time constant after stimulus onset, we speculate that the mechanism may explain how computation can spread rapidly through the hierarchical networks of the brain: The time window corresponds to one activation per binary neuron on average, which would correspond to only one spike per active biological neuron, similar to the fast feed-forward processing latencies measured experimentally in cortical areas [68, 69]. This shows how networks employing discrete communication can compute rapidly on the basis of a few single spikes instead of having the necessity to obtain an average spike rate.

E. Implications for noise and chaotic dynamics in cortex

Chaos on the individual spike level is a subject that has attracted considerable interest theoretically [14, 19, 23] and experimentally [70, 71]. Because the chaos transition is reached already for small network sizes N and weak synapse strengths g for binary neurons, it seems probable that biological networks in cortex, which have local sizes of $\mathcal{O}(10^3 - 10^5)$ neurons with similar correlation transmission curves as the binary model, operate in a regime of strong chaos on the single spike level. However, let us assume that notwithstanding, the spike times are close to the edge of chaos or not chaotic. This could be due to a specific connectivity motif that imposes an additional contractive effect onto state space. Also, the architecture would need to be robust enough against internal noise such as synaptic stochasticity and external noise, for example due to unrelated input from other brain areas. In such a case, spike-time dependent coding seems likely, since rate coding would be less efficient. Conversely, let us now assume that spike times are indeed chaotic. Then one possibility is that they are still used for effectively representing information despite chaos, as, for example, in the transient dimensionality expansion mechanism described above, or in the framework proposed by [72, 73].

The other possibility is that the quantity supporting computation are not the spike times, but an aggregated observable like spike packets or the spike rate. This quantity could then be tuned to the edge of chaotic dynamics to optimize computational power. This possibility underlies the idea of searching for a transition to firing-rate chaos in spiking networks [17, 20–22]. In such a case, the coding relevant firing rate is realized by a train of spikes with fully chaotic inter-spike intervals, which therefore constitute an intrinsic and effectively independent noise that is expected to degrade computational performance (although it has been argued that noise can be beneficial by aiding exploration of solution space [74] or stochastic resonance [75–77]). It is important to distinguish between frozen noise (where the realization is kept fixed), which suppresses chaos [25, 26] and can for example be

conceptualized as deterministic external input, and independent noise, which also has the suppressive effect but of course also results in a high variability of responses to stimuli.

For binary networks, we have shown that the effective discretization noise is so strong that it always suppresses chaos on the rate level. We expect that this generalizes to spiking networks with low firing rates, since then the binary neuron can be interpreted as behaving like a Poisson-spiking neuron, which should therefore have similar effective noise strength. By this argument, no transition to rate chaos in spiking networks is predicted by the classical rate network model [16]. Instead, the rate fluctuations that can be observed in simulated spiking networks should have origins not directly related to the chaos transition of rate networks, as indeed seems to be the case [17, 20–22]. Strongly fluctuating states are either caused by interactions between different populations, or the intrinsic membrane potential dynamics of the spiking neuron [78].

Also, to the best of our knowledge, there is so far no theoretical analysis of the computational capacities of a network displaying edge-of-chaos rate fluctuations in the presence of independent noise. While such a situation could certainly have arisen in the context of Liquid-state machines [65], a theoretical analysis would provide better a understanding of computation with firing rates in a spiking network.

Conclusion

We studied networks with continuous and discrete models of neural signaling in a unifying neuron-model independent framework derived from concepts of field theory. While the statistics of activity is well comparable across the models of neural communication, there are apparent differences in the dynamical behavior controlling their chaos transitions. This makes the generalization of results on chaos in rate networks to discrete or spiking networks a multifaceted story. In the chaotic regime, binary networks show a fast transient dimensionality increase of their stimulus representation, leading to fast and noise resilient computational abilities.

Acknowledgements

This work was partially supported by the Helmholtz young investigator’s group VH-NG-1028, the European Union’s Horizon 2020 research and innovation programme under grant agreement No. 785907 (Human Brain Project SGA2), the Exploratory Research Space (ERS) seed fund neuroIC002 (part of the DFG excellence initiative) of the RWTH university and the JARA Center for Doctoral studies within the graduate School for Simulation and Data Science (SSD).

1. Model-independent mean-field theory for random networks

This section presents a self-contained derivation of the model-independent mean-field theory for networks with Gaussian random connectivity $J_{ij} \stackrel{\text{i.i.d.}}{\sim} \mathcal{N}\left(\frac{\bar{g}}{N}, \frac{g^2}{N}\right)$. The N neurons have inputs $\mathbf{h}(t) = (h_1(t), \dots, h_N(t))$ and outputs $\mathbf{x}(t) = (x_1(t), \dots, x_N(t))$ and the neuronal dynamics is described by the conditional probability functional $\rho[x_i|h_i]$. For deterministic neurons, where $x_i = f[h_i]$ is some causal functional of the input, one may set $\rho[x_i|h_i] = \delta[x_i - f[h_i]]$. We use vectorial notation to denote

$$\rho[\mathbf{x}|\mathbf{h}] = \prod_{i=1}^N \rho[x_i|h_i],$$

because, given their inputs $\{h_i\}$, neurons are otherwise pairwise independent. The probability functional $\rho[x_i|h_i]$ is assumed to be strictly causal, which is $x_i(t)$ is independent of $h_i(s > t)$; a more explicit notation would be $\rho[x_i(\circ+)|h_i(\circ)]$, denoting that the time-argument $x_i(t+\epsilon)$ must be infinitesimally advanced by $\epsilon > 0$ compared to the argument of $h_i(t)$ for ρ not to vanish.

The joint statistics of input and output is then

$$\rho[\mathbf{x}, \mathbf{h}] = \rho[\mathbf{x}|\mathbf{h}] \rho[\mathbf{h}]. \quad (21)$$

The distribution of the inputs \mathbf{h} is given as the marginalization over \mathbf{x} as

$$\begin{aligned} \rho[\mathbf{h}] &= \int \mathcal{D}\mathbf{x} \rho[\mathbf{x}, \mathbf{h}] \\ &= \int \mathcal{D}\mathbf{x} \rho[\mathbf{x}|\mathbf{h}] \rho[\mathbf{h}]. \end{aligned} \quad (22)$$

The connectivity \mathbf{J} couples the outputs \mathbf{x} of the neurons to the input \mathbf{h} as

$$\mathbf{h}(t) = \mathbf{J} \mathbf{x}(t).$$

So in the marginalization (22) over \mathbf{x} we need to set

$$\begin{aligned} \rho[\mathbf{h}] &= \rho[\mathbf{h}(\circ)|\mathbf{x}(\circ)] = \delta[\mathbf{h} - \mathbf{J}\mathbf{x}] \\ &= \int \mathcal{D}\hat{\mathbf{h}} \exp(\hat{\mathbf{h}}^T \mathbf{h}) \exp(-\hat{\mathbf{h}}^T \mathbf{J}\mathbf{x}), \end{aligned} \quad (23)$$

where the path integral measure is $\int \mathcal{D}\hat{\mathbf{h}} = \prod_t \int_{-\infty}^{\infty} \frac{d\hat{h}_i(t)}{2\pi i}$ and the inner product is meant as $\hat{\mathbf{h}}^T \mathbf{h} = \sum_{i=1}^N \int_{-\infty}^{\infty} dt \hat{h}_i(t) h_i(t)$. By connecting the outputs back to the inputs, (21) may seem to take a circular structure like $\rho[\mathbf{x}, \mathbf{h}] = \rho[\mathbf{x}|\mathbf{h}] \rho[\mathbf{h}|\mathbf{x}]$. But since the first conditional probability is causal, and the second couples only equal time points, (21) is more accurately represented as

$$\rho[\mathbf{x}, \mathbf{h}] = \rho[\mathbf{x}(\circ+)|\mathbf{h}(\circ)] \rho[\mathbf{h}(\circ)|\mathbf{x}(\circ)]$$

which is ordered in time, resulting in a spiraling structure.

Performing the disorder average $\langle \dots \rangle_{\mathbf{J}}$ of (22), the only term affected is the last exponential factor in the second line of (23), which yields

$$\begin{aligned} &\left\langle \exp(-\hat{\mathbf{h}}^T \mathbf{J}\mathbf{x}) \right\rangle_{\mathbf{J} \stackrel{\text{i.i.d.}}{\sim} \mathcal{N}\left(\frac{\bar{g}}{N}, \frac{g^2}{N}\right)} \\ &= \exp\left(-\frac{\bar{g}}{N} \sum_{i=1}^N \hat{h}_i^T \sum_{j=1}^N x_j + \frac{g^2}{2N} \sum_{i,j=1}^N (\hat{h}_i^T x_j)^2\right). \end{aligned} \quad (24)$$

Here, we redefined the scalar product such that the last term in the exponent rewrites explicitly as

$$(\hat{h}_i^T x_j)^2 = \iint dt ds \hat{h}_i(t) \hat{h}_i(s) x_j(t) x_j(s).$$

This suggests the introduction of the auxiliary fields $\mathcal{R}(t) := \frac{\bar{g}}{N} \sum_j x_j(t)$ and $\mathcal{Q}(t, s) := \frac{g^2}{N} \sum_j x_j(t) x_j(s)$ to rewrite (24) as

$$\prod_i \exp\left(-\hat{h}_i^T \mathcal{R} + \frac{1}{2} \hat{h}_i^T \mathcal{Q} \hat{h}_i\right), \quad (25)$$

where the bi-linear form is to be read as

$$\hat{h}_i^T \mathcal{Q} \hat{h}_i = \iint dt ds \hat{h}_i^T(t) \mathcal{Q}(t, s) \hat{h}_i(s).$$

The appearance of the product sign and the neuron-independent fields \mathcal{R} and \mathcal{Q} signifies that the problem becomes completely symmetric with regard to neurons. Enforcing the definitions of the auxiliary fields by Dirac distributions, represented in Fourier domain analogous to (23), yields another pair of fields $\hat{\mathcal{R}}$ and $\hat{\mathcal{Q}}$ and brings (22) into the form

$$\begin{aligned} \langle \rho[\mathbf{h}] \rangle_J &\stackrel{(22),(23)}{=} \int \mathcal{D}\mathbf{x} \rho[\mathbf{x}|\mathbf{h}] \langle \delta[\mathbf{h} - \mathbf{J}\mathbf{x}] \rangle_J \\ &\stackrel{(24),(25)}{=} \int \mathcal{D}\{\mathcal{Q}, \mathcal{R}, \hat{\mathcal{Q}}, \hat{\mathcal{R}}\} \exp\left(-\frac{N}{\bar{g}} \hat{\mathcal{R}}^T \mathcal{R} - \frac{N}{g^2} \hat{\mathcal{Q}}^T \mathcal{Q}\right) \\ &\quad \times \prod_i \int \mathcal{D}\{x_i, \hat{h}_i\} \rho[x_i|h_i] \exp\left(\hat{h}_i^T h_i - \hat{h}_i^T \mathcal{R} + \frac{1}{2} \hat{h}_i^T \mathcal{Q} \hat{h}_i + \hat{\mathcal{R}}^T x_i + x_i^T \hat{\mathcal{Q}} x_i\right). \end{aligned} \quad (26)$$

We now compute the values of the auxiliary fields that provide the dominant contribution to the probability mass. To this end consider

$$\begin{aligned} 1 &\equiv \int \mathcal{D}\mathbf{h} \langle \rho[\mathbf{h}] \rangle_J \\ &\stackrel{(26)}{=} \int \mathcal{D}\{\mathcal{Q}, \mathcal{R}, \hat{\mathcal{Q}}, \hat{\mathcal{R}}\} \exp\left(-\frac{N}{\bar{g}} \hat{\mathcal{R}}^T \mathcal{R} - \frac{N}{g^2} \hat{\mathcal{Q}}^T \mathcal{Q}\right) \\ &\quad \times \prod_i \int \mathcal{D}\{x_i, h_i, \hat{h}_i\} \rho[x_i|h_i] \exp\left(\hat{h}_i^T h_i - \hat{h}_i^T \mathcal{R} + \frac{1}{2} \hat{h}_i^T \mathcal{Q} \hat{h}_i + \hat{\mathcal{R}}^T x_i + x_i^T \hat{\mathcal{Q}} x_i\right). \end{aligned}$$

The exponent in the second line can be considered an action of a field theory for the auxiliary fields $\{\mathcal{Q}, \mathcal{R}, \hat{\mathcal{Q}}, \hat{\mathcal{R}}\}$. The integral in the last line appears to the power of N , so that one may rewrite it as

$$\begin{aligned} &\int \mathcal{D}\{\mathcal{Q}, \mathcal{R}, \hat{\mathcal{Q}}, \hat{\mathcal{R}}\} \exp\left(N \Omega[\mathcal{R}, \mathcal{Q}, \hat{\mathcal{R}}, \hat{\mathcal{Q}}]\right) \\ \text{with } \Omega[\mathcal{R}, \mathcal{Q}, \hat{\mathcal{R}}, \hat{\mathcal{Q}}] &:= -\frac{\mathcal{R}^T \hat{\mathcal{R}}}{\bar{g}} - \frac{\mathcal{Q}^T \hat{\mathcal{Q}}}{g^2} \\ &\quad + \ln \int \mathcal{D}\{x, h, \hat{h}\} \rho[x|h] \exp\left(\hat{h}^T h - \hat{h}^T \mathcal{R} + \frac{1}{2} \hat{h}^T \mathcal{Q} \hat{h} + \hat{\mathcal{R}}^T x + x^T \hat{\mathcal{Q}} x\right). \end{aligned}$$

The appearance of N in the exponent $N \Omega[\mathcal{R}, \mathcal{Q}]$ suggests to perform the integration over the fields $\{\mathcal{Q}, \mathcal{R}, \hat{\mathcal{Q}}, \hat{\mathcal{R}}\}$ in saddle point approximation, demanding $\frac{\delta \Omega}{\delta \{\mathcal{Q}, \mathcal{R}, \hat{\mathcal{Q}}, \hat{\mathcal{R}}\}} \stackrel{!}{=} 0$, which yields four conditions for the saddle point values R, Q, \hat{R}, \hat{Q} of the field

$$\begin{aligned} R(t) &= \bar{g} \langle x(t) \rangle_{\Omega(R, Q)}, \\ \hat{R}(t) &= \bar{g} \langle \hat{h}(t) \rangle_{\Omega(R, Q)} \equiv 0, \\ Q(t, s) &= g^2 \langle x(t) x(s) \rangle_{\Omega(R, Q)}, \\ \hat{Q}(t, s) &= \frac{g^2}{2} \langle \hat{h}(t) \hat{h}(s) \rangle_{\Omega(R, Q)} \equiv 0. \end{aligned}$$

Here the expectation value is $\langle \dots \rangle_{\Omega(R, Q)} = \int \mathcal{D}\mathbf{x} \dots \int \mathcal{D}\{h, \hat{h}\} \rho[x|h] \exp\left(\hat{h}^T h - \hat{h}^T R + \frac{1}{2} \hat{h}^T Q \hat{h}\right)$. The outer derivative of \ln appearing in the expression for Ω vanishes, because the normalization condition of the latter distribution is unity, since the exponential term is the moment-generating functional of a Gaussian process $h \sim \mathcal{N}(R, Q)$ and $\rho[x|h]$ is normalized, allowing us to rewrite

$$\langle \dots \rangle_{\Omega(R, Q)} = \int \mathcal{D}\mathbf{x} \dots \langle \rho[x|h] \rangle_{h \sim \mathcal{N}(R, Q)}. \quad (27)$$

The auxiliary fields \hat{h} are zero on expectation, which is a consequence of the normalization [32, 36, Section X].

This leads to the result in the main text, eqs. (3) and (3).

2. Derivation of the ODE for autocorrelations in binary networks

We here derive equations (8) and (10) for the evolution of the autocorrelation.

To this end it is useful to perform a mapping from the Ising representation $x \in [-1, 1]$ of the binary state to the bit-like representation $n \in [0, 1]$ as

$$x = 2n - 1. \quad (28)$$

The correlation functions are correspondingly related as

$$\begin{aligned} q_I(t, s) &:= \langle x(t)x(s) \rangle \\ &= \langle (2n(t) - 1)(2n(s) - 1) \rangle \\ &= 4(\langle n(t)n(s) \rangle - \langle n(t) \rangle + 1), \end{aligned} \quad (29)$$

where by $Q(t, s) = g^2 q_I(t, s)$ we obtain the quantity considered in the main text, e.g. in (8). Defining $q(t, s) := \langle n(t)n(s) \rangle$ we have

$$\begin{aligned} q(t, s) &= \int dh \rho(h) \sum_{n(t)=0,1} \sum_{n(s)=0,1} n(t)n(s) \rho[n(t), n(s)|h] \\ &= \langle \rho[n(t) = 1, n(s) = 1|h] \rangle_{h \sim \rho}. \end{aligned} \quad (30)$$

where we write $\langle \dots \rangle_{h \sim \rho}$ as a short form of $\int dh \rho(h) \dots$. The latter joint probability is decomposed, analogous to (1), as

$$\rho[n(t) = 1, n(s) = 1|h] = \rho[x(t) = 1|x(s) = 1, h] \rho[x(s) = 1|h]. \quad (31)$$

We obtain the first conditional probability on the right by considering the possibilities to reach the final state $x(t) = 1$ given that $x(s) = 1$

$$\begin{aligned} \rho[x(t) = 1|x(s) = 1, h] &= P(\text{no updates in } (s, t)) \\ &\quad + P(\text{last update in } (s, t) \text{ to up-state}) \\ &= e^{-\frac{t-s}{\tau}} \\ &\quad + \int_s^t e^{-\frac{t-t'}{\tau}} T_p(h(t')) \frac{dt'}{\tau}. \end{aligned} \quad (32)$$

Likewise we obtain the latter conditional probability on the right of (31) as

$$\rho[x(s) = 1|h] = \int_{-\infty}^s e^{-\frac{s-t'}{\tau}} T_p(h(t')) \frac{dt'}{\tau}. \quad (33)$$

Combining (30), (32) and (33) we get

$$\begin{aligned} q(t, s) &= \left\langle \int_{-\infty}^s e^{-\frac{s-t'}{\tau}} T_p(h(t')) \frac{dt'}{\tau} \left(e^{-\frac{t-s}{\tau}} + \int_s^t e^{-\frac{t-t''}{\tau}} T_p(h(t'')) \frac{dt''}{\tau} \right) \right\rangle_{h \sim \rho} \\ &= \int_{-\infty}^s e^{-\frac{t-t'}{\tau}} \langle T_p(h(t')) \rangle_{h \sim \rho} \frac{dt'}{\tau} \\ &\quad + \int_{-\infty}^s e^{-\frac{s-t'}{\tau}} \int_s^t e^{-\frac{t-t''}{\tau}} \langle T_p(h(t')) T_p(h(t'')) \rangle_{h \sim \rho} \frac{dt''}{\tau} \frac{dt'}{\tau}. \end{aligned}$$

In the stationary state, the integral in the penultimate line reduces to $\langle T_p(h) \rangle_{h \sim \rho} e^{-\frac{t-s}{\tau}}$. Also $q(t, s) =: q(t-s)$ is then a function of the time lag $\Delta t := t - s$ alone

$$q(\Delta t) = \langle T_p(h) \rangle_{h \sim \rho} e^{-\frac{\Delta t}{\tau}} + \int_{-\infty}^s e^{-\frac{s-t'}{\tau}} \int_s^{s+\Delta t} e^{-\frac{s+\Delta t-t''}{\tau}} \langle T_p(h(t')) T_p(h(t'')) \rangle_{h \sim \rho} \frac{dt''}{\tau} \frac{dt'}{\tau}.$$

Differentiating by Δt we get

$$\begin{aligned} \tau \frac{d}{d\Delta t} q(\Delta t) &= -q(\Delta t) + \int_{-\infty}^s e^{-\frac{s-t'}{\tau}} \langle T_p(h(t')) T_p(h(s+\Delta t)) \rangle_{h \sim \rho} \frac{dt'}{\tau} \\ &= -q(\Delta t) + \int_0^\infty e^{-\frac{t}{\tau}} \langle T_p(h(0)) T_p(h(t+\Delta t)) \rangle_{h \sim \rho} \frac{dt}{\tau}, \end{aligned} \quad (34)$$

where we substituted $s - t' \rightarrow t$ in the last step and used the stationarity to shift the time arguments of the h by s . Using (28), (29), and (5) and assuming stationarity we get the result (10) in the main text, where the gain function T instead of T_p appears. Shifting the integration variable t by Δt , we obtain

$$\tau \frac{d}{d\Delta t} q(\Delta t) = -q(\Delta t) + \int_{\Delta t}^{\infty} e^{-\frac{t-\Delta t}{\tau}} \langle T_p(h(0)) T_p(h(t)) \rangle_{h \sim \rho} \frac{dt}{\tau}$$

and performing another derivative $\tau \frac{d}{d\Delta t}$ yields

$$\begin{aligned} \tau^2 \frac{d^2}{d\Delta t^2} q(\Delta t) &= -\tau \frac{d}{d\Delta t} q(\Delta t) + \int_{\Delta t}^{\infty} e^{-\frac{t-\Delta t}{\tau}} \langle T_p(h(0)) T_p(h(t)) \rangle_{h \sim \rho} \frac{dt}{\tau} \\ &\quad - \langle T_p(h(0)) T_p(h(\Delta t)) \rangle_{h \sim \rho} \\ &= q(\Delta t) - \langle T_p(h(0)) T_p(h(\Delta t)) \rangle_{h \sim \rho}, \end{aligned} \quad (35)$$

where for the second equality, we used the first-order differential equation. Closing the equation in the mean-field approximation, amounts to setting the measure of $h \sim \rho \equiv \mathcal{N}(R, Q)$ to the Gaussian process with mean R and variance Q , as determined by the saddle point equations by (2) and (3). This neglects fluctuations of \mathcal{R} and \mathcal{Q} . In App 3 we briefly discuss when this is justified.

Moving to the $[-1, 1]$ representation by using (28), (29), and (5) and multiplying (35) by g^2 changes $T_p \rightarrow T$ and $g^2 q \rightarrow Q$ so that we obtain (8). Here, in addition, we introduce $\mathcal{N}_{R, Q_0, Q}$ as the bivariate Gaussian with stationary mean R and covariance matrix $\begin{pmatrix} Q_0 & Q \\ Q & Q_0 \end{pmatrix}$. This allows us to employ Price's theorem [41] which states that

$$\frac{d}{dQ} \langle \mathcal{T}(h) \mathcal{T}(h') \rangle_{(h, h') \sim \mathcal{N}_{R, Q(0), Q}} \stackrel{(\text{Price's theorem})}{=} \langle T(h) T(h') \rangle_{(h, h') \sim \mathcal{N}_{R, Q(0), Q}},$$

where $\mathcal{T}(x) := \int^x T(x') dx'$ is the primitive of T .

3. Non-vanishing mean connectivity and negligibility of cross-correlations

Above, we identified the input autocorrelation with the scaled output autocorrelation. When cross-correlations vanish in the thermodynamic limit, this is justified. For vanishing mean connectivity, this is obviously true, but what happens if the mean connectivity is not zero? Remember that we consider the case of the average connectivity given by \bar{g}/N , as in the classical work by Sherrington and Kirkpatrick [79]. Then, the input fluctuations are given by

$$\langle h_i^2 \rangle - \langle h \rangle^2 = g^2 \langle x \rangle^2 + \bar{g}^2 \left(1 - \frac{1}{N} \right) c_{\#} + \left(\frac{\bar{g}^2}{N} + g^2 \right) \langle \langle x^2 \rangle \rangle \quad (36)$$

$$= g^2 \langle x^2 \rangle + \frac{\bar{g}^2}{N} \langle \langle x^2 \rangle \rangle + \bar{g}^2 \left(1 - \frac{1}{N} \right) c_{\#}, \quad (37)$$

where we introduced the average output cross-correlation between neurons $c_{\#}$. The first term of (37) is the raw second moment of the outputs times g^2 , as it appears for vanishing mean connectivity. The second term is obviously of order $1/N$. For the last term, this is less evident, because it requires the computation of output cross-correlations. However, it was demonstrated by Helias *et al.* [80], that for inhibitory feedback, these are of order $1/N$ as well. The derivation of this statement is lengthy, so that we limit ourselves to derive their equation (2) within our formalism to demonstrate how it allows the self-contained treatment of the $\bar{g} \neq 0$ -theory. From the generalization of (33) to two neurons, we obtain the self-consistent equation for the raw pairwise output cross-correlation

$$\langle x_i(t) x_j(t) \rangle = \int_{-\infty}^t \frac{dt'}{\tau} \int_{-\infty}^t \frac{dt''}{\tau} e^{-\frac{t-t'}{\tau}} e^{-\frac{t-t''}{\tau}} \langle T_p(h_i(t') - \Theta) T_p(h_j(t'') - \Theta) \rangle \quad (38)$$

$$\begin{aligned} \frac{d}{dt} \langle x_i(t) x_j(t) \rangle &= -2 \langle x_i(t) x_j(t) \rangle + \left\langle T_p(h_i(t) - \Theta) \int_{-\infty}^t \frac{dt''}{\tau} e^{-\frac{t-t''}{\tau}} T_p(h_j(t'') - \Theta) \right\rangle \\ &\quad + \left\langle \int_{-\infty}^t \frac{dt'}{\tau} e^{-\frac{t-t'}{\tau}} T_p(h_i(t') - \Theta) T_p(h_j(t) - \Theta) \right\rangle \end{aligned} \quad (39)$$

This looks nearly identical to [81, eq. (2)], from which [80, eq. (2)] can be derived - only the output variables multiplying the activation functions in the expectation values in [81, eq. (2)] are here replaced by

$$x'_i(t) := \int_{-\infty}^t \frac{dt'}{\tau} e^{-\frac{t-t'}{\tau}} T_p(h_i(t') - \Theta).$$

To evaluate the expression (39), we compute the correlation of this quantity with x_i :

$$\begin{aligned} \langle x_i(t) x'_i(t) \rangle &= \left\langle x_i(t) \int_{-\infty}^t \frac{dt'}{\tau} e^{-\frac{t-t'}{\tau}} T_p(h_i(t') - \Theta) \right\rangle = \left\langle \int_{-\infty}^t \frac{dt'}{\tau} e^{-\frac{t-t'}{\tau}} T_p(h_i(t') - \Theta) \right\rangle = \langle x_i(t) \rangle \\ \langle x_j(t) x'_i(t) \rangle &= \left\langle x_j(t) \int_{-\infty}^t \frac{dt'}{\tau} e^{-\frac{t-t'}{\tau}} T_p(h_i(t') - \Theta) \right\rangle \\ &= \left\langle \int_{-\infty}^t \frac{dt'}{\tau} e^{-\frac{t-t'}{\tau}} T_p(h_i(t') - \Theta) \int_{-\infty}^t \frac{dt''}{\tau} e^{-\frac{t-t''}{\tau}} T_p(h_i(t'') - \Theta) \right\rangle \stackrel{(38)}{=} \langle x_j(t) x_i(t) \rangle, \end{aligned}$$

where the first line holds true because $x'_i(t)$ gives the probability that $x_i(t) = 1$ and therefore, multiplying $x'_i(t)$ by $x_i(t)$ and taking the average yields the same as averaging just $x'_i(t)$. A similar reasoning holds for the cross-correlations in the second line: the updating process is independent for two distinct neurons, given the history of the inputs. Therefore, inside the average, we can replace $x_j(t)$ by the probability (given the input history) that neuron j is updated into state 1. Thus, the joint second order statistics of x' and x is identical to that of x and therefore (39) is equivalent to [81, eq. (2)], from which the results of [80] follow.

Especially, we conclude that for inhibition-dominated networks, the correlations are of order $1/N$ and therefore do not contribute to the input variance in the thermodynamic limit. Because the activity gets bistable for $\bar{g} > 1$ and fluctuates around one of two minima, where the feedback is inhibitory again, this mechanism persists in this case, too. Only close to the critical state $\bar{g} = 1$, correlations get large and violate the assumption of $1/N$ -scaling.

Summarizing, a mean connectivity of order $\mathcal{O}(1/N)$ in the thermodynamic limit and sufficiently far away from the critical point directly only affects the mean activity. The influence on the second cumulant is only indirect, analogous to a shift of the threshold, and not direct via additional contributions to the fluctuations of the input. This explains why the theory in Section II E fits the simulation data so well despite the neglect of cross-correlations.

4. Replica calculation for chaos

Model-independent replica calculation To assess the transition to chaos, we need to perform a replica calculation that considers a pair of networks with identical connectivity but slightly different initial conditions for the neurons. We use superscripts (1) and (2) to distinguish the two systems. The correlation between the two replica is a measure of the distance between their respective states in terms of the Euclidean distance

$$\begin{aligned} d^{(12)}(t) &:= \|\mathbf{x}^{(1)}(t) - \mathbf{x}^{(2)}(t)\|^2 \\ &= \sum_{\alpha=1}^2 \sum_{i=1}^N x_i^{(\alpha)} x_i^{(\alpha)} - 2 \sum_{i=1}^N x_i^{(1)} x_i^{(2)}. \end{aligned} \tag{40}$$

The first term, on expectation over realizations of the activity, approaches the average autocorrelation in the two replica and the latter term the inter-replica correlation. For Ising spins the expression simplifies to $2N - 2 \sum_{i=1}^N x_i^{(1)} x_i^{(2)}$.

The formal derivation of mean-field equations that approximate these quantities proceeds analogous to Section 1: The analog expression to (22) and (23) reads

$$\rho[\mathbf{h}^{(1)}, \mathbf{h}^{(2)}] = \int \mathcal{D}\{\mathbf{x}^{(1)}, \mathbf{x}^{(2)}\} \rho[\mathbf{x}^{(1)}, \mathbf{x}^{(2)} | \mathbf{h}^{(1)}, \mathbf{h}^{(2)}] \prod_{\alpha=1}^2 \delta[\mathbf{h}^{(\alpha)} - \mathbf{J} \mathbf{x}^{(\alpha)}].$$

Here the conditional density $\rho[\mathbf{x}^{(1)}, \mathbf{x}^{(2)} | \mathbf{h}^{(1)}, \mathbf{h}^{(2)}]$ is a joint distribution across the two replica, because it must allow the representation of update processes or stochastic activations of corresponding neurons that have identical realizations between the two replica.

The important point is the identical matrix \mathbf{J} appearing in the product of the latter two Dirac distributions, which,

after introducing Fourier representations as in (23) and taking the disorder average over \mathbf{J} , analogous to (24), yields

$$\begin{aligned} & \left\langle \exp \left(-\hat{\mathbf{h}}^{(1)\text{T}} \mathbf{J} \mathbf{x}^{(1)} - \hat{\mathbf{h}}^{(2)\text{T}} \mathbf{J} \mathbf{x}^{(2)} \right) \right\rangle_{\mathbf{J}^{\text{i.i.d.}} \mathcal{N}(\frac{\bar{g}}{N}, \frac{g^2}{N})} \\ &= \prod_{i=1}^N \prod_{\alpha=1}^2 \exp \left(-\frac{\bar{g}}{N} \hat{h}_i^{(\alpha)\text{T}} \sum_{j=1}^N x_j^{(\alpha)} + \frac{g^2}{2N} \sum_{j=1}^N (\hat{h}_i^{(\alpha)\text{T}} x_j^{(\alpha)})^2 \right) \\ & \quad \times \exp \left(\frac{g^2}{N} \sum_{j=1}^N \hat{h}_i^{(1)\text{T}} x_j^{(1)} \hat{h}_i^{(2)\text{T}} x_j^{(2)} \right). \end{aligned}$$

The penultimate line is the same contribution for each replica as in the single system; it is treated in the same manner by introducing pairs of auxiliary fields $\{\mathcal{R}^{(\alpha)}, \hat{\mathcal{R}}^{(\alpha)}, \mathcal{Q}^{(\alpha\beta)}, \hat{\mathcal{Q}}^{(\alpha\beta)}\}_{\alpha \in \{1,2\}}$. The last line couples the two replica and can be decoupled similarly by defining

$$\mathcal{Q}^{(12)}(t, s) := \frac{g^2}{N} \sum_{j=1}^N x_j^{(1)}(t) x_j^{(2)}(s).$$

This definition is enforced by inserting a δ -constraint, represented as a Fourier integral with the corresponding conjugate field $\hat{\mathcal{Q}}^{(12)}(s, t)$. The integral over $\{\mathcal{R}^{(\alpha)}, \hat{\mathcal{R}}^{(\alpha)}, \mathcal{Q}^{(\alpha\beta)}, \hat{\mathcal{Q}}^{(\alpha\beta)}\}_{\alpha, \beta \in \{1,2\}}$ is then taken in saddle point approximation with the resulting non-trivial saddle point equations

$$\begin{aligned} R^{(\alpha)}(t) &= \bar{g} \langle x^{(\alpha)}(t) \rangle_{\Omega(\{R^{(\alpha)}, Q^{(\alpha\beta)}\})}, \\ Q^{(\alpha\beta)}(t, s) &= g^2 \langle x^{(\alpha)}(t) x^{(\beta)}(s) \rangle_{\Omega(\{R^{(\alpha)}, Q^{(\alpha\beta)}\})}. \end{aligned} \quad (41)$$

The remaining $\hat{\mathcal{Q}}$ -fields all vanish $\hat{R}^{(\alpha)} = \hat{Q}^{(\alpha\beta)} \equiv 0$. The expectation value in (41) is taken with the measure

$$\langle \dots \rangle_{\Omega(\{R^{(\alpha)}, Q^{(\alpha\beta)}\})} = \int \mathcal{D}\{x^{(1)}, x^{(2)}\} \dots \langle \rho[x^{(1)}, x^{(2)} | h^{(1)}, h^{(2)}] \rangle_{(h^{(1)}, h^{(2)}) \sim \mathcal{N}(\{R^{(\alpha)}, Q^{(\alpha\beta)}\})}, \quad (42)$$

where $\mathcal{N}(\{R^{(\alpha)}, Q^{(\alpha\beta)}\})$ is a pair of Gaussian processes with cumulants

$$\begin{aligned} \langle\langle h^{(\alpha)}(t) \rangle\rangle &= R^{(\alpha)}(t), \\ \langle\langle h^{(\alpha)}(t) h^{(\beta)}(s) \rangle\rangle &= Q^{(\alpha\beta)}(t, s). \end{aligned}$$

The distance (40) between replica in mean-field approximation can then be written as

$$d^{(12)}(t) = g^{-2} \left(\sum_{\alpha=1}^2 Q^{(\alpha\alpha)}(t, t) - 2 Q^{(12)}(t, t) \right).$$

Application to binary networks The zero-lag cross-replica correlation is then given with (41) and (42) as

$$Q^{(12)}(t, t) \stackrel{(41,42)}{=} g^2 \sum_{x^{(1)}(t), x^{(1)}(t)=-1}^1 x^{(1)} \cdot x^{(2)} \langle \rho(x^{(1)}, x^{(2)}, t | h^{(1)}, h^{(2)}) \rangle_{(h^{(1)}, h^{(2)}) \sim \mathcal{N}(\{R^{(\alpha)}, Q^{(\alpha\beta)}\})}.$$

To construct $\rho(x^{(1)}, x^{(2)}, t | h^{(1)}, h^{(2)})$, first note that both neurons are updated by the same stochastic realizations of the update process. This process has two random components: The drawing of the update time point t' , which, for the Poisson updates, has a distribution of $e^{-\frac{t-t'}{\tau}} \frac{dt'}{\tau}$ for the next event to come in $[t', t' + dt]$, and the stochastic activation depending on the gain function $T_p \in [0, 1]$, whose value for both replica is compared to the same realization of a uniformly distributed random number $r \in [0, 1]$.

The four possible outcomes of this update of states $(x^{(1)}, x^{(2)})$ are $(-1, -1)$, $(1, 1)$, both of which lead to $x^{(1)} \cdot x^{(2)} = +1$ and $(-1, 1)$, $(1, -1)$, both of which lead to $x^{(1)} \cdot x^{(2)} = -1$. One thus only needs to distinguish two outcomes: The event $x^{(1)} \cdot x^{(2)} = -1$ takes place if the random variable r is in between the values of the two gain functions, $T_p(h^{(1)}) < r < T_p(h^{(2)})$, which happens with probability $p_{\text{diff}} = |T_p(h^{(1)}) - T_p(h^{(2)})|$; the other event $x^{(1)} \cdot x^{(2)} = +1$ with $1 - p_{\text{diff}}$. So in total we get at the time t' of update

$$\begin{aligned} \langle x^{(1)}(t') x^{(2)}(t') \rangle_r &= (-1) \cdot p_{\text{diff}} + (+1) \cdot (1 - p_{\text{diff}}) \\ &= 1 - 2 p_{\text{diff}} = 1 - 2 |T_p(h^{(1)}(t')) - T_p(h^{(2)}(t'))|. \end{aligned} \quad (43)$$

Taken together with the asynchronous update time point, we thus have

$$Q^{(12)}(t, t) = g^2 \int_{-\infty}^t \frac{dt'}{\tau} e^{-\frac{t-t'}{\tau}} \left(1 - 2 \langle |T_p(h^{(1)}(t')) - T_p(h^{(2)}(t'))| \rangle_{(h^{(1)}, h^{(2)}) \sim \mathcal{N}(\{R^{(\alpha)}, Q^{(\alpha\beta)}\})} \right).$$

Taking a derivative with respect to t , we obtain an ODE governing the time evolution of the cross-replica correlation

$$\tau \frac{d}{dt} Q^{(12)}(t, t) = -Q^{(12)}(t, t) + g^2 \left(1 - 2 \langle |T_p(h^{(1)}(t)) - T_p(h^{(2)}(t))| \rangle_{(h^{(1)}, h^{(2)}) \sim \mathcal{N}(\{R^{(\alpha)}, Q^{(\alpha\beta)}\})} \right). \quad (44)$$

Note that $Q^{(12)}(t)$ also appears implicitly in the distribution of $h^{(1)}, h^{(2)}$, rendering the equation nonlinear. This derives the result (12) in the main text, which follows by replacing $2(T_p(h^{(1)}) - T_p(h^{(2)})) = T(h^{(1)}) - T(h^{(2)})$ due to (5).

So far we have proceeded without approximation. Perfect correlation of the replicas $Q^{(12)}(t, t) = Q_0 = g^2$ is clearly a fixed point, since then $h^{(1)}(t) = h^{(2)}(t)$ and the right hand side vanishes. We now wish to assess the stability of this solution, that is, whether a perturbation of one replica results in recovery of perfect correlation (regular dynamics) or in a decorrelation of the replicas (chaos). Making the ansatz $Q^{(12)}(t, t) = Q_0 - \epsilon(t)$ and using the mean field approximation of the input distribution, the last term of the ODE (44) becomes, by substituting $H := \frac{h^{(1)} + h^{(2)}}{2}$, $h := \frac{h^{(1)} - h^{(2)}}{2}$ and then expanding in h and $\epsilon/2Q_0$:

$$\begin{aligned} & \langle |T_p(h^{(1)}) - T_p(h^{(2)})| \rangle_{(h^{(1)}, h^{(2)}) \sim \mathcal{N}\left(\begin{pmatrix} R \\ R \end{pmatrix}, \begin{pmatrix} Q_0 & Q_0 - \epsilon \\ Q_0 - \epsilon & Q_0 \end{pmatrix}\right)} \\ &= \langle |T_p(H + h) - T_p(H - h)| \rangle_{(H, h) \sim \mathcal{N}\left(\begin{pmatrix} R \\ 0 \end{pmatrix}, \begin{pmatrix} Q_0 - \frac{\epsilon}{2} & 0 \\ 0 & \frac{\epsilon}{2} \end{pmatrix}\right)} \\ &= \frac{1}{2\pi\sqrt{\frac{\epsilon}{2}(Q_0 - \frac{\epsilon}{2})}} \int \int \exp\left(-\frac{H^2}{2(Q_0 - \frac{\epsilon}{2})} - \frac{h^2}{2\frac{\epsilon}{2}}\right) \\ & \quad \times |T_p(R + H + h) - T_p(R + H - h)| dH dh \\ &= \frac{1}{2\pi\sqrt{\frac{\epsilon}{2}(Q_0 - \frac{\epsilon}{2})}} \int \int e^{-\frac{H^2}{2(Q_0 - \frac{\epsilon}{2})}} e^{-\frac{h^2}{\epsilon}} |2T'_p(R + H)h + \mathcal{O}(h^3)| dH dh \\ &= 2 \cdot \frac{1}{\sqrt{2\pi Q_0}} \int e^{-\frac{H^2}{2Q_0}} |T'_p(R + H)| dH \frac{1}{\sqrt{2\pi\frac{\epsilon}{2}}} \int |h| e^{-\frac{h^2}{\epsilon}} dh (1 + \mathcal{O}(\epsilon)) \\ &= 2 \langle T'_p(H) \rangle_{H \sim \mathcal{N}(R, Q_0)} \sqrt{\frac{\epsilon}{\pi}} + \mathcal{O}\left(\epsilon^{\frac{3}{2}}\right). \end{aligned} \quad (45)$$

Plugging this result and the ansatz $Q^{(12)}(t) = Q_0 - \epsilon(t)$ back into (44) then yields (13).

5. Fluxtubes in binary networks

It has been shown by Touzel and Wolf [53] that the borders of fluxtubes in spiking networks of inhibitory LIF-neurons are related to changes in the global order of spikes. In particular, if a perturbation creates an additional spike or causes the omission of an expected one, the mean firing rate will stay constant but the order of future spikes is very likely to be irrevocably changed. The divergence rate of two trajectories can be assessed by calculating the mean number of unexpected spike order changes caused by a single such perturbation, resulting in a branching process. In the context of our binary networks, we can ask the equivalent question: Given a flip of a single neuron's activity variable, how many 'wrong' update results will occur on average in the following time τ ?

The flip of one neuron $x_j \rightarrow -x_j$ causes a change $\Delta h_i = -2J_{ij}x_j$ in the input of neurons it is connected to. Across different target neurons Δh is therefore distributed as

$$\rho(\Delta h) = \mathcal{N}\left(\pm 2\frac{\bar{g}}{N}, 4\frac{g^2}{N}\right)$$

and the probability of a neuron to be updated into the wrong state due to the perturbation in the input is

$$p(\text{flip}(x)|\Delta h) = \langle |T_p(h + \Delta h) - T_p(h)| \rangle_{h \sim \mathcal{N}(R, Q_0)} \stackrel{|\Delta h| \ll 1, T'_p \geq 0}{\approx} |\Delta h| \langle T'_p(h) \rangle_{h \sim \mathcal{N}(R, Q_0)},$$

where the absolute value enters because both directions of perturbation cause a positive probability of 'wrong' updating, and we assumed $T' \geq 0$ for simplicity. Now we ask the question how many downstream flips n_{spawns} will, on average, be triggered in the network during one time constant, given a single original flip. This quantity controls whether the decorrelating flips will proliferate or not, because since every neuron is updated on average once per time constant, if $n_{\text{spawns}} < 1$ and the neuron carrying the original flip is updated again, it is most likely updated 'correctly' again and the average number of flips in the network has decreased. If $n_{\text{spawns}} > 1$ on the other hand, the average number of flips increases.

Being interested in the transition point, we can assume $n_{\text{spawns}} \approx 1$ so that we do not need to take the interaction of several flips into account. Then

$$\bar{n}_{\text{spawns}} = N \langle p(\text{flip}(x)|\Delta h) \rangle_{\Delta h} \quad (46)$$

and while we take the mean input R into account, we neglect the mean perturbing input $\langle \Delta h \rangle = \pm 2\bar{g}/N = \mathcal{O}(N^{-1}) \approx 0$ as it is small compared to the standard deviation $\sigma_{\Delta h} = 2g/\sqrt{N} = \mathcal{O}(N^{-\frac{1}{2}})$, allowing the simple calculation

$$\begin{aligned} \bar{n}_{\text{spawns}} &= N \langle T'_p(h) \rangle_{h \sim \mathcal{N}(R, Q_0)} \langle |\Delta h| \rangle_{\Delta h \sim \mathcal{N}(0, \sigma_{\Delta h}^2)} \\ &= N \langle T'_p(h) \rangle_{h \sim \mathcal{N}(R, Q_0)} \sqrt{\frac{2}{\pi}} \sigma_{\Delta h} \\ &= 2\sqrt{\frac{2N}{\pi}} g \langle T'_p(h) \rangle_{h \sim \mathcal{N}(R, Q_0)}. \end{aligned}$$

Finally, accounting for $T'_p(h) = T'(h)/2$, given by (5), the chaos transition is expected at

$$1 \stackrel{!}{=} \bar{n}_{\text{spawns}} = \frac{\sqrt{2N}}{\sqrt{\pi}} g \langle T'(h) \rangle_{h \sim \mathcal{N}(R, Q_0)}, \quad (47)$$

which is exactly the result (15), derived via the completely different route of the replica calculation. While the derivation here is nicely and intuitively interpretable, the derivation via field theory and replica calculation allows for systematic generalizations. For example, it is not clear how to obtain the residual correlation (14) in the ad-hoc approach.

Fluxtube size.

The fluxtube diameter is not a very informative measure for a binary network, since the system trajectory in phase space is typically not in the middle of a 'tube' but close to some of its boundaries (given by the thresholds). Therefore, the distance to a boundary strongly depends on the direction of perturbation. As a relatively informative measure, we consider smearing the trajectory in all directions with some variance $\text{Var}(\Delta h) = \sigma_{\text{fl}}^2$, which is chosen such that on average, one fluxtube boundary is crossed. This procedure makes sense in so far, as it is similar to adding noise onto the input. It is important to be aware that σ_{fl} is not strictly the average distance to the closest boundary, although the two quantities should covary.

The situation is analogous to the above calculation, because we again need to consider the flips occurring during an update in (on average) all N neurons, which is given by (46) only with $\sigma_{\Delta h}$ replaced by σ_{fl} . Demanding $\bar{n}_{\text{spawns}} \stackrel{!}{=} 1$ then yields

$$\begin{aligned} 1 &\stackrel{!}{=} N \langle p(\text{flip}(x)|\Delta h) \rangle_{\Delta h \sim \mathcal{N}(0, \sigma_{\text{fl}}^2)} \\ \Rightarrow \quad \sigma_{\text{fl}} &= \frac{\sqrt{2\pi}}{N \langle T'(h) \rangle_{h \sim \mathcal{N}(R, Q_0)}}. \end{aligned}$$

Of course, the $1/N$ scaling needs to be taken with caution, since our perturbation goes into all N phase space directions, resulting in a total length scaling as $1/\sqrt{N}$.

6. Slope of correlation transmission in binary and rate neurons

We here show that the difference between discrete signaling and continuous signaling leads to a qualitative difference in the slope of the correlation-transmission curve and thus the transition to chaos.

Assume, as an approximation, that two neurons receive inputs that are jointly Gaussian distributed as

$$(h_1, h_2) \sim \mathcal{N}(0, K),$$

where the covariance matrix is given by

$$K(c_{\text{in}}) := q \begin{pmatrix} 1 & c_{\text{in}} \\ c_{\text{in}} & 1 \end{pmatrix}.$$

Here $c_{\text{in}} \in [-1, 1]$ controls the correlation between the inputs.

Continuous signaling A neuron with continuous signaling has the output

$$y_i = T(h_i),$$

where $T \in [-1, 1]$ is an activation function. The mean output is thus

$$\langle y_i \rangle = \langle T(h) \rangle_{h \sim \mathcal{N}(0, q)}. \quad (48)$$

For a point symmetric gain function that we assume in the following the mean vanishes so that the variance of the outputs is

$$a = \langle T^2(h) \rangle_{h \sim \mathcal{N}(0, q)}.$$

The correlation coefficient between the outputs of a pair of neurons is

$$\begin{aligned} c_{\text{out}}^{\text{cont.}}(c_{\text{in}}) &:= a^{-1} \langle y_1 y_2 \rangle \\ &= a^{-1} \langle T(h_1) T(h_2) \rangle_{(h_1, h_2) \sim \mathcal{N}(0, K(c_{\text{in}}))} \end{aligned} \quad (49)$$

which has the slope

$$\frac{dc_{\text{out}}^{\text{cont.}}(c_{\text{in}})}{dc_{\text{in}}} = a^{-1} \langle T'(h_1) T'(h_2) \rangle_{(h_1, h_2) \sim \mathcal{N}(0, K(c_{\text{in}}))},$$

by Price's theorem [41]. Evaluated at $c_{\text{in}} = 1$ this is

$$\frac{dc_{\text{out}}^{\text{cont.}}(1)}{dc_{\text{in}}} = a^{-1} \langle (T'(h))^2 \rangle_{h \sim \mathcal{N}(0, q)} \stackrel{T' < \infty}{<} \infty. \quad (50)$$

For activation functions T with finite slope $T' < \infty$ this slope is thus finite. For the signum function $T(x) = 2H(x) - 1$ we get $a = 1$ and

$$\begin{aligned} \frac{dc_{\text{out}}^{\text{cont.}}(c_{\text{in}})}{dc_{\text{in}}} &= 2 \langle \delta(h_1) \delta(h_2) \rangle_{(h_1, h_2) \sim \mathcal{N}(0, K(c_{\text{in}}))} \\ &= \frac{1}{\pi \sqrt{\det(K(c_{\text{in}}))}} = (q\pi)^{-1} (1 - c_{\text{in}}^2)^{-\frac{1}{2}}, \end{aligned} \quad (51)$$

where the latter line comes from the normalization condition of the two-dimensional Gaussian distribution. Thus, the slope diverges if and only if the output of the neuron becomes discrete.

Discrete signaling Now consider a neuron with discrete output, but smooth activation function $T \in [-1, 1]$; a smooth function here corresponds to a probabilistic activation

$$y_i = \begin{cases} 1 & \text{with prob. } (T(h) + 1)/2 \\ -1 & \text{with prob. } 1 - (T(h) + 1)/2 \end{cases}.$$

The mean output is thus

$$\begin{aligned} \langle y_i \rangle &= \langle 1 \cdot (T(h) + 1)/2 - 1 \cdot (1 - (T(h) + 1)/2) \rangle_{h \sim \mathcal{N}(0, q)} \\ &= \langle T(h) \rangle_{h \sim \mathcal{N}(0, q)}, \end{aligned}$$

the same as for the continuous signaling (48). For a point symmetric gain function that we assume in the following the mean vanishes so that the variance of the outputs is $a = 1$.

The correlation coefficient of the output is then identical to the second moment between the outputs of a pair of neurons

$$\begin{aligned} c_{\text{out}}^{\text{disc}}(c_{\text{in}}) &:= \langle y_1 y_2 \rangle \\ &= 1 \cdot (1 - p_{\text{diff}}) - 1 \cdot p_{\text{diff}} = 1 - 2p_{\text{diff}} \\ &= 1 - \langle |T(h_1) - T(h_2)| \rangle_{(h_1, h_2) \sim \mathcal{N}(0, K(c_{\text{in}}))}. \end{aligned} \quad (52)$$

The latter expression is related to the probability $p_{\text{diff}} = \frac{1}{2} \langle |T(h_1) - T(h_2)| \rangle$ that the two neurons are in different states. This expression is of course the same as found in (45). In the limit of $c_{\text{in}} \rightarrow 1$ we thus have

$$c_{\text{out}}^{\text{disc}}(c_{\text{in}}) \stackrel{c_{\text{in}}=1-\hat{\epsilon}}{\simeq} 1 - 2 \langle T'(h) \rangle_{h \sim \mathcal{N}(0, q)} \sqrt{\frac{\hat{\epsilon}}{\pi}} + \mathcal{O}(\hat{\epsilon}^{3/2})$$

where $\hat{\epsilon} = \frac{\epsilon}{g^2}$. So the slope diverges for $c_{\text{in}} \rightarrow 1$ as

$$\begin{aligned} \left. \frac{dc_{\text{out}}^{\text{disc}}(c_{\text{in}})}{dc_{\text{in}}} \right|_{c_{\text{in}}=1-\hat{\epsilon}} &\stackrel{(45)}{=} \frac{d}{d(-\hat{\epsilon})} \left[1 - 2 \langle T'(h) \rangle_{h \sim \mathcal{N}(0, q)} \sqrt{\frac{\hat{\epsilon}}{\pi}} + \mathcal{O}(\hat{\epsilon}^{3/2}) \right] \\ &= \langle T'(h) \rangle_{h \sim \mathcal{N}(0, q)} (\pi \hat{\epsilon})^{-\frac{1}{2}} + \mathcal{O}(\hat{\epsilon}^{1/2}) \\ &\propto (1 - c_{\text{in}})^{-\frac{1}{2}}. \end{aligned}$$

This divergence is present even if the gain function is finite $T' < \infty$, in contrast to the finite slope found for the continuous signaling in (50).

The infinite slope for continuous signaling in the limit of a sharp activation function, (51), moreover, has a different form of divergence for $c_{\text{in}} \rightarrow 1$.

7. Noisy binary pattern classification task

We implement a classification task by training one linear readout

$$S_{\alpha'}(t) = w_{\alpha'}(t)^T (x_{\alpha}(t) + \xi_{\text{pre}}) + \xi_{\text{post}} \quad (53)$$

of the network state $x_{\alpha}(t)$ at time t for each of the $\alpha' = 1, \dots, P = 50$ patterns to be detected. Here ξ_{pre} and ξ_{post} are additional Gaussian readout noises of standard deviation $\sigma_{\xi, \text{pre}}$ and $\sigma_{\xi, \text{post}}$. ξ_{pre} controls how precisely a single neuron's state can be read out. ξ_{post} represents a noise component of the readout mechanism. Training of the readout $w_{\alpha'}(t)$ is performed for each time point t by linear regression (see App 7 a), minimizing the quadratic error of detecting the stimulus identity, i.e. minimizing $(S_{\alpha'} - \delta_{\alpha\alpha'})^2$.

The patterns are presented to the network by initializing the first $L = 10$ of the $N = 500$ neurons to the stimulus. All other neurons are in an initial state corresponding to the stationary statistics. Each stimulus α is a random binary pattern of length L with $\{-1, 1\}$ appearing equally likely, superimposed with Gaussian noise of standard deviation σ . The resulting evolution of the network state, given this initial condition, is termed $x_{\alpha}(t)$.

a. Linear regression

Minimizing the quadratic error over all patterns amounts to linear regression; we consider a single scalar readout target value $y_{\alpha} \in \mathbb{R}$ for each pattern α ; in the example above $y_{\alpha} \in \{0, 1\}$. Then $w, x \in \mathbb{R}^N$ and the quadratic error is

$$\epsilon := \min_w \sum_{\alpha=1}^P (w^T x_{\alpha} - y_{\alpha})^2. \quad (54)$$

Demanding stationarity with regard to w by differentiating by ∂_{w_i} we get N equations

$$\begin{aligned} 0 &= \sum_{\alpha=1}^P 2 (w^T x_{\alpha} - y_{\alpha}) x_{\alpha i} \quad \forall i \\ w^T \sum_{\alpha=1}^P x_{\alpha} x_{\alpha}^T &= \sum_{\alpha=1}^P y_{\alpha} x_{\alpha}^T. \end{aligned}$$

The value w^* to achieve stationarity is

$$w^* = C^{-1} \sum_{\alpha=1}^P y_{\alpha} x_{\alpha}, \quad (55)$$

$$\text{with } C := \sum_{\alpha=1}^P x_{\alpha} x_{\alpha}^T,$$

where we used the symmetry of C . Inserted into (54)

$$\begin{aligned} \epsilon &= w^{*\text{T}} C w^* - 2 w^{*\text{T}} \sum_{\alpha} y_{\alpha} x_{\alpha} + \sum_{\alpha} y_{\alpha}^2 \\ &= \sum_{\alpha=1}^P y_{\alpha}^2 - S, \\ S &= \left(\sum_{\alpha=1}^P y_{\alpha} x_{\alpha}^T \right) C^{-1} \left(\sum_{\alpha=1}^P y_{\alpha} x_{\alpha} \right). \end{aligned} \quad (56)$$

In the case of classification, the latter expression simplifies even further: the first term is a constant $\sum_{\alpha=1}^P y_{\alpha}^2 = 1$ for labels $y_{\alpha} \in \{0, 1\}$, where $y_{\alpha} = 1$ if the presented pattern α is the pattern α' to be detected and $y_{\alpha} = 0$ else, $y_{\alpha} = \delta_{\alpha\alpha'}$. The second term is then identical to the definition (53) for $\xi = 0$, obtained by inserting w^* from (55). The expression shows that the signal amplitude $S_{\alpha'}$ actually depends on the signal to noise ratio, the length of the selected vector $x_{\alpha'}$ measured with regard to the variability C across all patterns

$$S_{\alpha'} = x_{\alpha'}^T C^{-1} x_{\alpha'}. \quad (57)$$

The generalization to stochastic realizations of x_{α} , for example due to the presentation of noisy patterns is straight forward. We need to replace $\sum_{\alpha=1}^P \dots$ by $\sum_{\alpha=1}^P \langle \dots \rangle$ in the measure for the error (54) and thus throughout this calculation, where $\langle \dots \rangle$ is the expectation over the noise realizations.

b. Approximation of orthogonal patterns

If the patterns x are sufficiently orthogonal, we can think of the entries k of any state vector x_{α} to be drawn independently. So the $x_{\alpha,k} \in \{-1, 1\}$ appear with equal probability for those entries that lie in the subspace of dimension d_s . All remaining entries are assumed to be constant. We may thus restrict the space to the d_s informative components. The kl -th element of the covariance matrix for independently drawn entries is

$$\begin{aligned} C_{kl} &= \sum_{\alpha=1}^P x_{\alpha k} x_{\alpha l} \\ &\simeq P \delta_{kl}. \end{aligned} \quad (58)$$

The signal of the readout α' , following from (57), then takes the simple form

$$S_{\alpha'} \simeq P^{-1} \|x_{\alpha'}\|_{d_s}^2. \quad (59)$$

If the signal is perfectly reliable, that is, if for all noise realizations i the response $x_{\alpha i}$ is equal to the stereotypical response $x_{\alpha i} = \bar{x}_{\alpha}$, and if the dimension of the informative subspace is d_s , so $\bar{x} \in \mathbb{R}^{d_s}$, we get with $\|\bar{x}\|_{d_s}^2 = d_s$

$$S_{\alpha', \max} \lesssim \frac{d_s}{P}.$$

For responses that are not perfectly reliable, we need to replace $x_{\alpha'}$ by $\langle x_{\alpha'} \rangle$ in (57) and thus

$$S_{\alpha} \simeq P^{-1} \|\langle x_{\alpha'} \rangle\|_{d_s}^2.$$

c. Nonzero plateau of the signal.

In the simulations, the noise distance somewhat unintuitively saturates slightly below the signal distance. This is explainable by taking into account that not all the initial noise realizations actually cause a crossing of the fluxtube

boundary. Instead, those realizations simply follow the unperturbed pattern trajectory, so that $d_{n,i} = 0$ in those cases. Then it is clear that the average noise distance is smaller than the one predicted based on the assumption of diverging trajectories:

$$\langle d_{n,i} \rangle_i = (1 - p_{\text{no flip}}) d_n^{\text{residual}}.$$

We can estimate the probability that no flip occurred due to the noise by using the results from App 5, where we calculated the average number of flips in the network after one time constant given an additional (noise) variance in the input of the neurons $\sigma_{\Delta h}^2$. In our present case the noise is given by adding $\xi_i \sim \mathcal{N}(0, \sigma^2)$ on the output activities of the L original neurons of the pattern, so that the corresponding input variance felt by all neurons in the network is

$$\tilde{\sigma}_{\Delta h}^2 = \frac{g^2}{N} \sigma^2 L.$$

Now we only need to consider that actually the variance is not constant for a complete round of N updates, but linearly diminishes every time one of the L source neurons is updated until none is left. Since the flip-probability depends on the square root of the variance, there is a corrective factor $c_{\text{dim}} = \sqrt{1 - \frac{k}{N}}$ in each term of the product:

$$\begin{aligned} p_{\text{no flip}} &= \prod_{k=0}^{N-1} (1 - p_{\text{single flip}}(k)) \\ &= \prod_{k=0}^{N-1} \left(1 - \frac{1}{N} \bar{n}_{\text{spawns}} (\langle \Delta h^2 \rangle) c_{\text{dim}}(k) \right) \\ &= \prod_{k=0}^{N-1} \left(1 - g\sigma \sqrt{\frac{2L}{\pi N}} \langle T'_p(h) \rangle_{h \sim \mathcal{N}(R, Q_0)} \sqrt{1 - \frac{k}{N}} \right). \end{aligned}$$

8. Description of simulations

Simulations for Figure 2 and Figure 5b,d were implemented using NEST [82]. To do so, a little trick was necessary, because NEST treats binary neurons in the bit-like $\{0, 1\}$ representation. To let every neuron “see” inputs from $\{-1, 1\}$ Ising spins we added to each neuron i a bias $\sum_j J_{ij}$ and then connected the neurons by the connections $2J_{ij}$ instead of J_{ij} ; thereby effectively simulating an Ising system. To obtain the autocorrelations for the Ising case, (29) was used, leading to the result shown in Figure 2.

For Figure 5b and d, for each point of the grid one simulation of two identical networks was performed. After 1000 ms, in one replica, the first two neurons were set to the active and the third and fourth neurons set to the inactive state, after which simulation continued for 2500 ms. This method of perturbation entails the small probability that these 4 neurons were already in exactly this state, so that nothing is changed; this is the explanation for the scattered single green dots in Figure 5b,d. The advantage of the method was, however, that it guaranteed the same state of the random number generators across both replicas.

The simulations for Figure 6, Figure 7 and Figure 8 were performed using a custom Fortran kernel. Analysis of simulation data and numerical implementations used Python scripts. At the moment our code is only available upon request, but it will be made freely accessible upon publication.

-
- [1] I. Ginzburg and H. Sompolinsky, *Theory of correlations in stochastic neural networks*, Phys. Rev. E **50**, 3171 (1994).
 - [2] C. van Vreeswijk and H. Sompolinsky, *Chaos in neuronal networks with balanced excitatory and inhibitory activity*, Science **274**, 1724 (1996).
 - [3] D. J. Amit and N. Brunel, *Dynamics of a recurrent network of spiking neurons before and following learning*, Network: Comput. Neural Systems **8**, 373 (1997).
 - [4] N. Brunel, *Dynamics of sparsely connected networks of excitatory and inhibitory spiking neurons*, J. Comput. Neurosci. **8**, 183 (2000).
 - [5] A. Renart, J. De La Rocha, P. Bartho, L. Hollender, N. Parga, A. Reyes, and K. D. Harris, *The asynchronous state in cortical circuits*, Science **327**, 587 (2010).
 - [6] M. Okun and I. Lampl, *Instantaneous correlation of excitation and inhibition during sensory-evoked activities*, Nat. Neurosci. **11**, 535 (2008).

- [7] A. S. Ecker, P. Berens, G. A. Keliris, M. Bethge, and N. K. Logothetis, *Decorrelated neuronal firing in cortical microcircuits*, Science **327**, 584 (2010).
- [8] P. König, A. K. Engel, and W. Singer, *Integrator or coincidence detector? The role of the cortical neuron revisited*, TINS **19**, 130 (1996).
- [9] M. N. Shadlen and W. T. Newsome, *The variable discharge of cortical neurons: Implications for connectivity, computation, and information coding*, J. Neurosci. **18**, 3870 (1998).
- [10] M. N. Shadlen and A. J. Movshon, *Synchrony unbound: A critical evaluation of the temporal binding hypothesis*, Neuron **24**, 67 (1999).
- [11] E. T. Rolls and G. Deco, *The Noisy Brain: Stochastic Dynamics as a Principle* (Oxford University Press, 2010).
- [12] R. Brette, *Philosophy of the spike: Rate-based vs. spike-based theories of the brain*, Frontiers in Systems Neuroscience **9**, 151 (2015).
- [13] T. Toyozumi and L. F. Abbott, *Beyond the edge of chaos: Amplification and temporal integration by recurrent networks in the chaotic regime*, Phys. Rev. E **84**, 051908 (2011).
- [14] N. Bertschinger and T. Natschläger, *Real-time computation at the edge of chaos in recurrent neural networks*, Neural Comput. **16**, 1413 (2004).
- [15] R. Legenstein and W. Maass, *What makes a dynamical system computationally powerful?* in *New Directions in Statistical Signal Processing: From System to Brains*, edited by S. Haykin, J. C. Principe, T. J. Sejnowski, and J. G. McWhirter (MIT Press, 2007) pp. 127–154.
- [16] H. Sompolinsky, A. Crisanti, and H. J. Sommers, *Chaos in random neural networks*, Phys. Rev. Lett. **61**, 259 (1988).
- [17] O. Harish and D. Hansel, *Asynchronous rate chaos in spiking neuronal circuits*, PLoS Comput Biol **11**, e1004266 (2015).
- [18] J. Kadmon and H. Sompolinsky, *Transition to chaos in random neuronal networks*, Phys. Rev. X **5**, 041030 (2015).
- [19] L. Büsing, B. Schrauwen, and R. Legenstein, *Connectivity, dynamics, and memory in reservoir computing with binary and analog neurons*, Neural Comput. **22**, 1272 (2010).
- [20] S. Ostojic, *Two types of asynchronous activity in networks of excitatory and inhibitory spiking neurons*, Nat. Neurosci. **17**, 594 (2014).
- [21] R. Engelken, F. Farkhooi, D. Hansel, C. van Vreeswijk, and F. Wolf, *Comment on "two types of asynchronous activity in networks of excitatory and inhibitory spiking neurons"*, bioRxiv , 017798 (2015).
- [22] S. Ostojic, *Response to comment on "two types of asynchronous activity in networks of excitatory and inhibitory spiking neurons"*, bioRxiv , 020354 (2015).
- [23] M. Monteforte and F. Wolf, *Dynamic flux tubes form reservoirs of stability in neuronal circuits*, Phys. Rev. X , 041007 (2012).
- [24] A. Crisanti and H. Sompolinsky, *Path integral approach to random neural networks*, Phys Rev E **98**, 062120 (2018).
- [25] L. Molgedey, J. Schuchhardt, and H. Schuster, *Suppressing chaos in neural networks by noise*, Phys. Rev. Lett. **69**, 3717 (1992).
- [26] J. Schuecker, S. Goedeke, and M. Helias, *Optimal sequence memory in driven random networks*, Phys Rev X **8**, 041029 (2018).
- [27] C. van Vreeswijk and H. Sompolinsky, *Chaotic balanced state in a model of cortical circuits*, Neural Comput. **10**, 1321 (1998).
- [28] R. Glauber, *Time-dependent statistics of the Ising model*, J. Math. Phys. **4**, 294 (1963).
- [29] P. Martin, E. Siggia, and H. Rose, *Statistical dynamics of classical systems*, Phys. Rev. A **8**, 423 (1973).
- [30] C. De Dominicis, *Techniques de renormalisation de la théorie des champs et dynamique des phénomènes critiques*, J. Phys. Colloques **37**, C1 (1976).
- [31] J. A. Hertz, Y. Roudi, and P. Sollich, *Path integral methods for the dynamics of stochastic and disordered systems*, Journal of Physics A: Mathematical and Theoretical **50**, 033001 (2017).
- [32] M. Helias and D. Dahmen, *Statistical field theory for neural networks*, arXiv (2019), 1901.10416 [cond-mat.dis-nn].
- [33] M. Doi, *Second quantization representation for classical many-particle system*, Journal of Physics A: Mathematical and General **9**, 1465 (1976).
- [34] L. Peliti, *Path integral approach to birth-death processes on a lattice*, J. Phys. France , 1469 (1985).
- [35] H. Sommers, *Path-integral approach to ising spin-glass dynamics*, Phys. Rev. Lett. **58**, 1268 (1987).
- [36] A. C. C. Coolen, *Statistical mechanics of recurrent neural networks ii. dynamics*, arXiv:cond-mat/0006011 (2000).
- [37] M. A. Buice and J. D. Cowan, *Field-theoretic approach to fluctuation effects in neural networks*, Phys. Rev. E **75**, 051919 (2007).
- [38] H. Sompolinsky and A. Zippelius, *Dynamic theory of the spin-glass phase*, Phys. Rev. Lett. **47**, 359 (1981).
- [39] S. Kirkpatrick and D. Sherrington, *Infinite-ranged models of spin-glasses*, Phys. Rev. B **17**, 4384 (1978).
- [40] M. Mézard, G. Parisi, and M. Virasoro, *Spin Glass Theory and Beyond (World Scientific Lecture Notes in Physics, Vol 9)* (World Scientific Publishing Company, 1987).
- [41] A. Papoulis and S. U. Pillai, *Probability, Random Variables, and Stochastic Processes*, 4th ed. (McGraw-Hill, Boston, 2002).
- [42] K. Rajan, L. Abbott, and H. Sompolinsky, *Stimulus-dependent suppression of chaos in recurrent neural networks*, Phys. Rev. E **82**, 011903 (2010).
- [43] J. Aljadeff, M. Stern, and T. Sharpee, *Transition to chaos in random networks with cell-type-specific connectivity*, Phys. Rev. Lett. **114**, 088101 (2015).
- [44] D. Martí, N. Brunel, and S. Ostojic, *Correlations between synapses in pairs of neurons slow down dynamics in randomly connected neural networks*, Phys. Rev. E **97**, 062314 (2018).
- [45] D. Sussillo and L. F. Abbott, *Generating coherent patterns of activity from chaotic neural networks*, Neuron **63**, 544 (2009).

- [46] B. Derrida and Y. Pomeau, *Random networks of automata: a simple annealed approximation*, EPL (Europhysics Letters) **1**, 45 (1986).
- [47] T. Tetzlaff, M. Buschermöhle, M. Diesmann, and T. Geisel, in *Proceedings of the 29th Göttingen Neurobiology Conference* (2003) submitted.
- [48] T. Tetzlaff, M. Buschermöhle, T. Geisel, and M. Diesmann, *The spread of rate and correlation in stationary cortical networks*, Neurocomputing **52–54**, 949 (2003).
- [49] E. Shea-Brown, K. Josic, J. De la Rocha, and B. Doiron, *Universal properties of correlation transfer in integrate-and-fire neurons*, Arxiv:q-bio (2007).
- [50] E. Shea-Brown, K. Josic, J. de la Rocha, and B. Doiron, *Correlation and synchrony transfer in integrate-and-fire neurons: basic properties and consequences for coding*, Phys. Rev. Lett. **100**, 108102 (2008).
- [51] T. Tchumatchenko, A. Malyshev, T. Geisel, M. Volgushev, and F. Wolf, *Correlations and synchrony in threshold neuron models*, Phys. Rev. Lett. **104**, 058102 (2010).
- [52] T. Deniz and S. Rotter, *Solving the two-dimensional fokker-planck equation for strongly correlated neurons*, Physical Review E **95** (2017), 10.1103/physreve.95.012412.
- [53] M. P. Touzel and F. Wolf, *Statistical mechanics of spike events underlying phase space partitioning and sequence codes in large-scale models of neural circuits*, Physical Review E **99** (2019), 10.1103/physreve.99.052402.
- [54] S. Hwang, V. Folli, E. Lanza, G. Parisi, G. Ruocco, and F. Zamponi, *On the number of limit cycles in asymmetric neural networks*, Journal of Statistical Mechanics: Theory and Experiment **2019**, 053402 (2019).
- [55] D. Grytskyy, T. Tetzlaff, M. Diesmann, and M. Helias, *A unified view on weakly correlated recurrent networks*, Front. Comput. Neurosci. **7**, 131 (2013).
- [56] T. Tetzlaff, M. Helias, G. T. Einevoll, and M. Diesmann, *Decorrelation of neural-network activity by inhibitory feedback*, PLOS Comput. Biol. **8**, e1002596 (2012).
- [57] L. Kuśmierczak, S. Ogawa, and T. Toyoizumi, *Edge of chaos and scale-free avalanches in neural networks with heavy-tailed synaptic disorder*, arXiv (2019), arXiv:1910.05780.
- [58] A. C. C. Coolen, in *Neuro-Informatics and neural modelling*, edited by F. Moss and S. Gielen (2001) pp. 553–684.
- [59] B. Lindner, B. Doiron, and A. Longtin, *Theory of oscillatory firing induced by spatially correlated noise and delayed inhibitory feedback*, Phys. Rev. E **72**, 061919 (2005).
- [60] D. Grytskyy, T. Tetzlaff, M. Diesmann, and M. Helias, *Invariance of covariances arises out of noise*, AIP Conf. Proc. **1510**, 258 (2013).
- [61] T. Tetzlaff, A. Morrison, T. Geisel, and M. Diesmann, *Consequences of realistic network size on the stability of embedded synfire chains*, Neurocomputing **58–60**, 117 (2004).
- [62] T. Tchumatchenko, T. Geisel, M. Volgushev, and F. Wolf, *Spike correlations – what can they tell about synchrony?* Frontiers in Neuroscience **5** (2011), 10.3389/fnins.2011.00068.
- [63] M. Schultze-Kraft, M. Diesmann, S. Gruen, and M. Helias, *Noise suppression and surplus synchrony by coincidence detection*, PLOS Comput. Biol. **9**, e1002904 (2013).
- [64] S. A. Kauffman, *The Origins of Order Self-Organization and Selection in Evolution* (Oxford University Press, 1993).
- [65] R. Legenstein and W. Maass, *Edge of chaos and prediction of computational performance for neural circuit models*, Neural Networks **20**, 323 (2007).
- [66] V. N. Vapnik, *Adaptive and learning systems for signal processing communications, and control*, Statistical learning theory (1998).
- [67] D. Snyder, A. Goudarzi, and C. Teuscher, in *Artificial Life 13* (MIT Press, 2012).
- [68] S. Thorpe, D. Fize, and C. Marlot, *Speed of processing in the human visual system*, Nature **381**, 520 (1996).
- [69] C. P. Hung, G. Kreiman, T. Poggio, and J. J. DiCarlo, *Fast readout of object identity from macaque inferior temporal cortex*, Science **310**, 863 (2005).
- [70] M. London, A. Roth, L. Beeren, M. Häusser, and P. E. Latham, *Sensitivity to perturbations in vivo implies high noise and suggests rate coding in cortex*, Nature **466**, 123 (2010).
- [71] M. Nolte, M. W. Reimann, J. G. King, H. Markram, and E. B. Muller, *Cortical reliability amid noise and chaos*, Nature Communications **10**, 1 (2019).
- [72] M. Boerlin, C. K. Machens, and S. Denève, *Predictive coding of dynamical variables in balanced spiking networks*, PLoS Computational Biology **9**, e1003258 (2013).
- [73] S. Denève and C. K. Machens, *Efficient codes and balanced networks*, Nature Neuroscience **19**, 375 (2016).
- [74] W. Maass, *Noise as a resource for computation and learning in networks of spiking neurons*, Proc. IEEE **102**, 860 (2014).
- [75] K. Wiesenfeld and F. Jaramillo, *Minireview of stochastic resonance*, Chaos **8**, 539 (1998).
- [76] J. Mayor and W. Gerstner, *Noise-enhanced computation in a model of a cortical column*, NeuroReport **16**, 1237 (2005).
- [77] M. D. McDonnell and D. Abbott, *What is stochastic resonance? definitions, misconceptions, debates, and its relevance to biology*, PLOS Comput. Biol. **5**, e1000348. doi:10.1371/journal.pcbi.1000348 (2009).
- [78] B. Kriener, H. Enger, T. Tetzlaff, H. E. Plesser, M.-O. Gewaltig, and G. T. Einevoll, *Dynamics of self-sustained asynchronous-irregular activity in random networks of spiking neurons with strong synapses*, Front. Comput. Neurosci. **8**, 136 (2014).
- [79] D. Sherrington and S. Kirkpatrick, *Solvable model of a spin-glass*, Phys. Rev. Lett. **35**, 1792 (1975).
- [80] M. Helias, T. Tetzlaff, and M. Diesmann, *The correlation structure of local cortical networks intrinsically results from recurrent dynamics*, PLOS Comput. Biol. **10**, e1003428 (2014).
- [81] D. Dahmen, H. Bos, and M. Helias, *Correlated fluctuations in strongly coupled binary networks beyond equilibrium*, Phys Rev X **6**, 031024 (2016).

- [82] C. Linssen, M. E. Lepperød, J. Mitchell, J. Pronold, J. M. Eppler, C. Keup, A. Peyser, S. Kunkel, P. Weidel, Y. Nodem, D. Terhorst, R. Deepu, M. Deger, J. Hahne, A. Sinha, A. Antonietti, M. Schmidt, L. Paz, J. Garrido, T. Ippen, L. Riquelme, A. Serenko, T. Kühn, I. Kitayama, H. Mørk, S. Spreizer, J. Jordan, J. Krishnan, M. Senden, E. Hagen, A. Shusharin, S. B. Vennemo, D. Rodarie, A. Morrison, S. Graber, J. Schuecker, S. Diaz, B. Zajzon, and H. E. Plesser, Nest 2.16.0, (2018).